Pure appl. geophys. 166 (2009) 1369–1402
0033–4553/09/081369–34
DOI 10.1007/s00024-009-0504-3

Pure and Applied Geophysics

Sardinia Coastal Uplift and Volcanism

Patrizia Mariani,[1] Carla Braitenberg,[1] and Fabrizio Antonioli[2]

Abstract—The low variability of MIS 5.5 sea level (M.I.S = Marine Isotopic Stage) with respect to the present day sea level, allows the Sardinian coast to be used as an eustatic reference for the entire Mediterranean region. This level is generally at 7 ± 2 m above current sea level along the Sardinian coast. One sector along the Orosei Gulf (eastern Sardinia) includes a characteristic and well conserved tidal notch that changes in elevation from 7.6 to 11.5 m over only 30 km, tilting upwards towards the north. Generally, height deviations of such a tidal notch would be due to tectonic or volcanic activity. The Sardinia coast however, is considered to have too little tectonic activity, and also too small post-glacial rebound in order to explain the anomaly. The remaining possibility is Neogene-Quaternary continental and/or submarine volcanic activity, which we investigate as a possible cause for the observed anomalies. In this paper, our goal is to explain the anomaly by modelling recent volcanic loading or updoming related to magmatic intrusion emplacement. We review the literature on the recent volcanic deposits, both on-shore and off-shore, and investigate to what extent volcanic loads can influence the coastline from a theoretical standpoint, using the isostatic flexure model and a range of loads. We find that the observed notch height anomaly cannot be explained by volcanic loading, but must be produced by an upward welling due to the emplacement of volcanic material, as produced for instance by a laccolith or batholith. The upward movement could be related to the submarine volcano only recently detected, or to a source located on the eastern Sardinia coast near Orosei.

Key words: Tyrrhenian notch, lithospheric flexure, volcanic intrusion, vertical crustal movements, Sardinia.

1. Introduction

The shoreline in southern Sardinia is considered to have been stable since the Early Miocene (Patacca *et al*., 1990; Gueguen *et al*., 1998). It is characterized by low seismic activity and no presently active volcanic activity (e.g., Ferranti *et al*., 2006; Finetti *et al*., 2005). The Plio-Quaternary volcanic deposits and the present seismic activity are illustrated in Figure 1A. An extensive number (58) of MIS 5.5 sites has been reported for Sardinia, with the distribution of markers mainly controlled by lithology, since most notches are found on limestone promontories. Inner margins are poorly identifiable at low lying coastal areas owing to the thick continental cover, which was not eroded due to the

[1] Department of Earth Sciences, University of Trieste, via Weiss 1, 34100 Trieste, Italy. E-mail: patrizia_mariani1979@yahoo.it; berg@units.it

[2] ENEA, Via Anguillarese 301, 00060 S.M. di Galeria Roma, Italy.

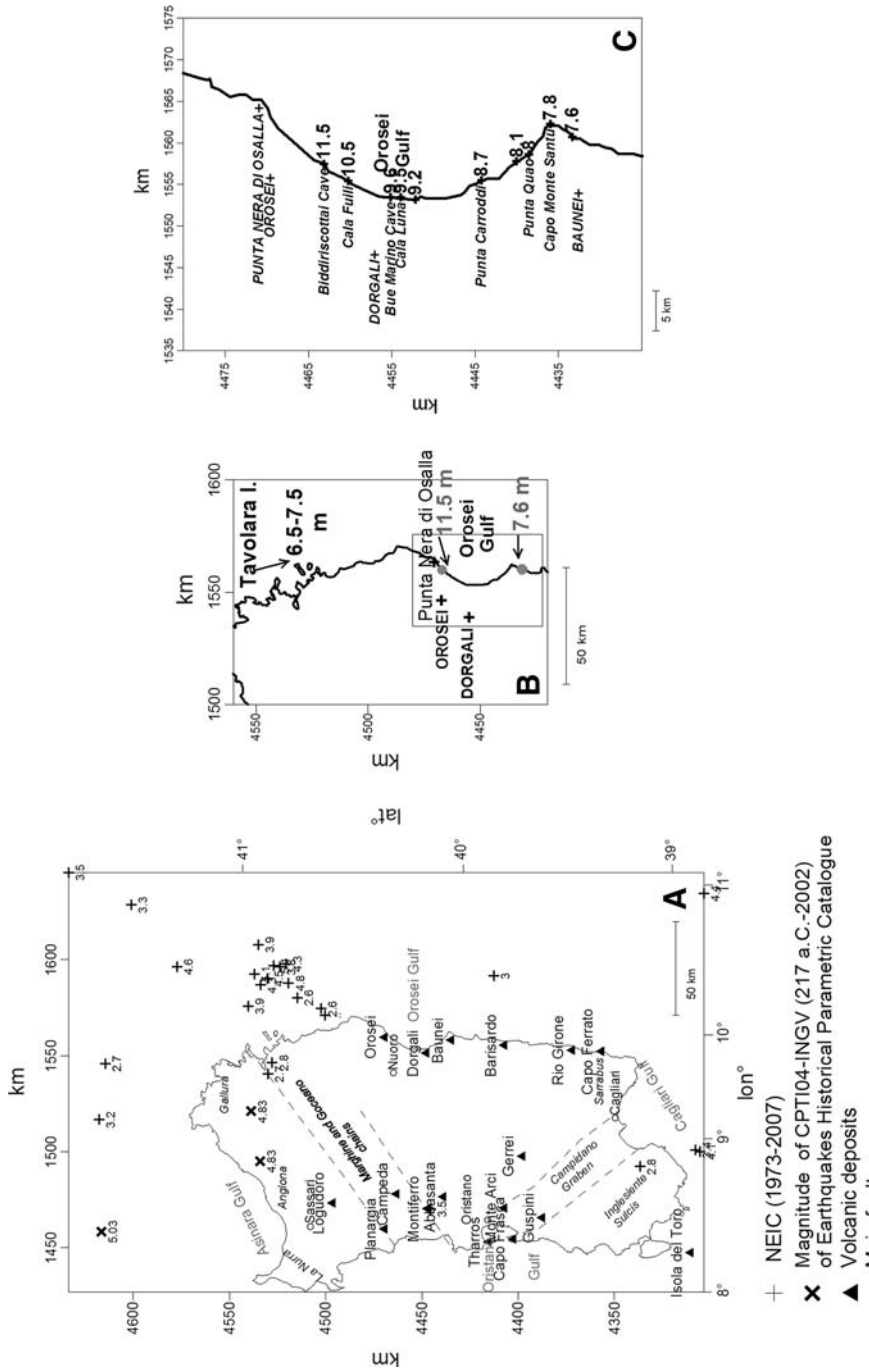
km
lon°
lat°
A
B
C
50 km
5 km
Tavolara I.
6.5-7.5 m
Punta Nera di Osalla
11.5 m
Orosei Gulf
7.6 m
OROSEI +
DORGALI +
PUNTA NERA DI OSALLA+
OROSEI+
Biddiriscottai Cave
11.5
Cala Fuili
10.5
DORGALI+
Bue Marino Cave
Cala Luna
9.6
9.5
Gulf
9.2
Orosei
Punta Carroddi
8.7
Punta Quaos
8.1
Capo Monte Santu
7.8
7.6
BAUNEI+
NEIC (1973-2007)
Magnitude of CPTI04-INGV (217 a.C.-2002) of Earthquakes Historical Parametric Catalogue
Volcanic deposits
Main faults

◀ Figure 1
Map of the Island of Sardinia:. A) Main tectonic units and seismicity. Magnitude of the seismic events is shown below the epicentre; rectangular area shows the coastal segment reported in Figure 1B; B) Height of the tidal notch of Tyrrhenian age (125 ka) along the northeastern coast; rectangular area shows the coastal segment reported in Figure 1C; (C) Coastal segment with elevated height of tidal notch along the Orosei Gulf. Height-values given in m above present sea level.

tectonically stable conditions of the island. Sardinia is the only region in the Tyrrhenian Sea where the marker elevation has a very low variability and is set at 8-10 m.

The joint presence of tectonic stability and limestone, the latter allowing the carving of the tidal notch of Tyrrhenian age (MIS 5.5, 125 ka), are the conditions for which this part of the Sardinian coastline has been chosen as the reference level of the Tyrrhenian (MIS 5.5) sea level for the central Mediterranean (LAMBECK *et al.*, 2004a, b; FERRANTI *et al.*, 2006).

It is therefore presumable, that the tidal notch should be found at the same altitude along the entire coast of the island, as no presently active tectonic, volcanic and anthropogenic sources generating a vertical movement are expected. This is the fact for most of the island, except along the Orosei Gulf, located in the central part of the eastern coast of the island (Figs. 1B, C), where a variation in the height of the notch of the order of 4 m has been detected, with the level increasing from north to south from 7.6 to 11.5 m (FERRANTI *et al.*, 2006; ANTONIOLI and TRAINITO, 2005). About 200 km north, on the limestone Tavolara Island, the altitude of the tidal notch is between 6.5 and 7.5 m, that is at the predicted eustatic values.

The tilting anomaly is preserved in only 30 km of the 70 km total length of the Orosei Gulf, where the lithology preserves the tidal notch. There is also a cover of sandstone and cementing sand that protected the notch from chemical dissolving by meteoric water during the post Tyrrhenian glacial age. Tidal notches (height = local tide) are especially well developed in many coastal zones of the Central Mediterranean Sea because of its microtidal regime: 0.37–0.4 m for sea-wave and air-pressure changes except for Tunisia and the Trieste area, which have larger (1–1.80 m) tidal ranges. Tidal notches therefore indicate episodes of sea-level relative stillstand (lower than 0.7 mm\yrs). At many Italian tectonically active coasts, where evidence exists of large current uplift (eastern Sicily) and subsidence (Trieste, north Adriatic Sea), the present-day marine notch is lacking because the tectonic rates are faster than the rate of carving. In Figure 2 we show a section of one of the longest Tyrrhenian notches and we compare it with the present tidal notch: The formation of the present tidal notch in the limestone lithology is an indicator of the actual regional stability of the island (KERSHAW and ANTONIOLI, 2004). The tidal notches are carved in the eastern Sardinia formation, composed by competent limestone series (formation 18b of geologic map of Sardinia, CONTI *et al.*, 1996). The form of the fossil as well as of the modern tidal notch is very well developed in the Orosei Gulf (the modern notch has a width of 55–80 cm and depth of concavity to 2 m. ANTONIOLI *et al.* (2006) attribute this effect to the presence of an efficient karst system close to the shoreline, which produced a powerful and sustained spring water flow (often of the order

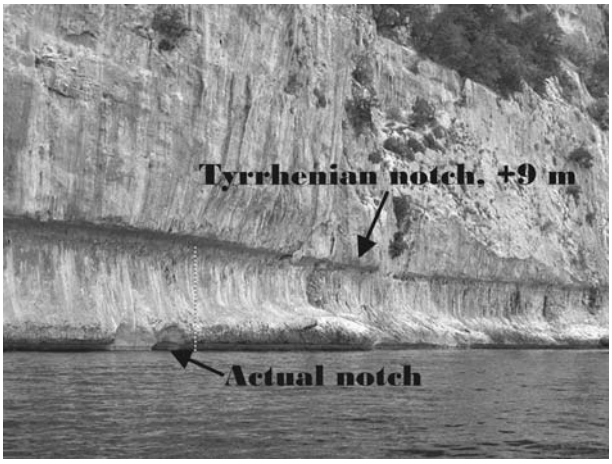

Figure 2
Section of the tidal notch of the Orosei Gulf, one of the longest tidal notch morphologies in the world. Actual notch is for the present day.

of 1–10 m^3/s). The continual presence of continental water (that floats on the marine water) has arguably increased the chemical dissolution processes at tide level.

According to many authors (Ferranti *et al.*, 2006; Assorgia *et al.*, 1997; Casula *et al.*, 2001) the northerly tilt of the Dorgali-Orosei notch is related to the isostatic response to residual Pliocene-Quaternary activity of the Dorgali-Orosei volcanic fields (location see Fig. 1A). In this work we intend to analyze this hypothesis in more detail and with quantitative methods.

For the purpose of our study, we summarize the past volcanic activity of the island and identify the different volcanic complexes. Particular attention is given to the age of the different complexes. As will be shown later, there are uncertainties regarding the ages of the volcanic extrusions, according to different authors. Concerning the offshore volcanic activity, no age determination can be found. Our summary shows in which parts of the island additional investigations are necessary to define the age of the volcanic extrusions. The existing literature discusses the geochemistry of the volcanism in some detail, but does not define the ages of the deposits in sufficient resolution in time and space.

So as to study the vertical movement of the coastline in response to loading, we adopt the lithospheric flexure model (e.g., Watts, 2002) and investigate under what conditions a volcanic surface load can produce a downwelling and upwelling of the crust. The flexural response is investigated with a sensitivity analysis, by generating synthetic load models with variable geometrical dimensions and positions relative to the coast. In a second step, we investigate the possible volcanic loads that could have influenced the notch in question, including in the analysis the updoming of the crust due to an overpressure caused by a magmatic intrusion. In the course of our study we come to the

Table 1

Age (in Ma) of the last phase of activity for the main volcanic deposits in Sardinia, according to different authors. For Conti *et al. (1996), the numbering of the associated geological maps are used, comprised of the interval 0.14-5.3 Ma, of 5a = Pliocene, 5b = Plio-Pleistocene; 6 = Pliocene; n.r.a. = no radiometric (age) available*

VOLCANIC DEPOSITS	*AGE FROM DIFFERENT AUTHORS FOR THE VOLCANIC DEPOSITS*					
	Beccaluva *et al.* (1975)	Beccaluva *et al.* (1985)	Petteruti Lieberknecht *et al.* (2003)	Lustrino *et al.* (2004)	Lustrino *et al.* (2007b)	Conti *et al.* (1996)
CAPO FERRATO	3,9-Quaternary	5,0-5,3	5,9-5,0	5,9-5,0	6,65-5	5 a
MONTE ARCI	3,3-Quaternary	3,7-2,8	3,7-2,7	3,8-2,6	3,8-2,6	6, 5 a, 5 b
MONTIFERRO	3,9-Quaternary	3,9-1,6	3,8-2,3	3,9-1,6	3,9-1,6	5 b, 5 a
NORTH. B. PLAT.	3,9-Quaternary	3,8-1,7		3,1-2	3,7-3,5	5 b
SOUTH. B. PLAT.	3,9-Quaternary	3,8-1,7		3,8-2,1	3,8-2,1	5 b
LOGUDORO	3,9-Quaternary	2,4-1,8 + 0, 9- < 0,15	3,18-0,11	3,1-0,1	2,4-0,4	5 b
OROSEI-DORGALI	3,9-Quaternary	3,9-2,1	3,8-1,7	3,6-2	3,9-2,1	5 b
CAPO FRASCA	3,9-Quaternary		1.6	n.r.a.	n.r.a	5 b
THARROS	3,9-Quaternary			n.r.a	n.r.a	5 b
BARISARDO	3,9-Quaternary			n.r.a	n.r.a	5 b
RIOGIRONE				n.r.a	6,4	
GUSPINI					4.4	

conclusion that the surface volcanic loads, considering also their published ages (Table 1), are unable to generate the observed anomaly of the notch. We find that the upward movement of the notch could be explained by a magmatic intrusion. Our study implies that the volcanic activity on Sardinia reached into the late Pleistocene, and was not limited to the western side of the island, but affected also the north-eastern part.

2. *Volcanism in Sardinia*

In order to study the anomaly of the MIS 5.5 coastline level located along the Orosei Gulf, we considered as a possible cause Plio-Quaternary volcanism. Of particular interest for our discussion is the volcanism younger than 1 Ma, as the crustal response to a load reaches equilibrium after 10^5-10^6 years (Watts, 2002).

We have reviewed the existing literature regarding the extension and temporal evolution of the Sardinian volcanism, which allows us to make a synthesis of the magmatic-tectonic evolution model during Tertiary and Quaternary for Italy in general and Sardinia in particular. As will be shown, there are discrepancies within the literature which we discuss in the following.

A simplified palinspastic evolution in the Western Mediterranean is as follows. The middle Eocene (50 Ma) is characterized by compressional tectonics linked to the collision of the African (Gondwana) and the European (Laurasia) domains. During the Late

Oligocene - Early Miocene (∼30-15 Ma) the collision between the Briançonnais microplate (Sardo-Corso block) with the Apulian continental margin is associated with the westward subduction of oceanic crust (relict Tetide's Ionian Sea; Beccaluva *et al.*, 2004; Lustrino *et al.*, 2004; Speranza *et al.*, 2002) to produce the first Sardinian volcanic activity with the formation of a NE-SW and E-W oriented transpressive fault system in the Sardinian and Corsica Varisican basement (Carmignani *et al.*, 1992, 1994, 1995; Pasci, 1997). This effusive-explosive calcoalcaline volcanic phase (lavas and/or andesitic, rhyolitic, dacitic and basaltic ignimbrites) continued until the exhaustion of the compressional events. During the Burdingalian (Early Miocene) the tectonic conditions began to change from compressive to extensional as a result of the withdrawal of the subduction of the slab. At this time the counter-clockwise rotation (∼30° Carmignani *et al.*, 2004; 40° Speranza *et al.*, 1999) of the Sardinia-Corsica block occurred, that detaching from south of France and Spain, generated the Provençal and Balearic basins (first extensive event) and migration toward east of the Appeninic foreland (presently still active, Carmignani *et al.*, 2004). During the following ∼10 Ma there are no volcanic levels in Sardinia, but to the east the northern Tyrrhenian Sea formation began. From the late Tortonian (∼8 Ma) to the Quaternary (Kastens *et al.*, 1988; Sartori, 1989; Mascle and Rehault, 1990) the Sardinia-Corso Tyrrhenian margin was passive, due to the formation of the Tyrrhenian Sea. New $^{40}Ar/^{39}Ar$ dates (Lustrino *et al.*, 2007a, b) have established that the second Sardinian volcanic activity with the formation of "Plio-Quaternary volcanic rocks" (or the Miocene-Quaternary volcanic episode, Lustrino *et al.*, 2007a), began in the Middle Miocene ∼11.8 Ma and persisted until the upper Pleistocene (∼0.1–0.2 Ma). This extensive phase saw volcanism of anorogenic type, and the formation of Campidano Graben (Fig. 3A). It is characterized by fissural activity (Bigazzi *et al.*, 1971; Savelli and Pasini, 1973; Di Paola *et al.*, 1975; Savelli, 1975; Beccaluva *et al.*, 1977, 1985) and alkaline, transitional, calcalkaline affinity. At the same time, the evaporitic succession of Messinain Age (10-5 Ma) was deposited. The formation of Samassi (continental formation) ended the successive regression.

Summarizing, we may conclude that there were two volcanic phases in Sardinia, which according to Beccaluva *et al.* (2004) were linked to the geodynamic evolution of a singular subduction process:

1. Eocene-Oligocene subduction (orogenic emplacement of Oligo-Miocenic volcanic products, Figure 3A, unit 4 on the geological map): Sardinian volcanism linked to the subduction of Ionic oceanic lithosphere under the continental European paleo-margin, where this subduction is a consequence of the opening of the Sardinia-Corsica interarc basin and the rotation of the Sardinia-Corsica block.
2. Neogene-Quaternary subduction (intraplate anorogenic (Fig. 3A, unit 2), linked to Plio-Quaternary volcanism, induced by the tensional tectonics that characterized the adjacent Tyrrhenian area. This results in the intense production of magmatic activity

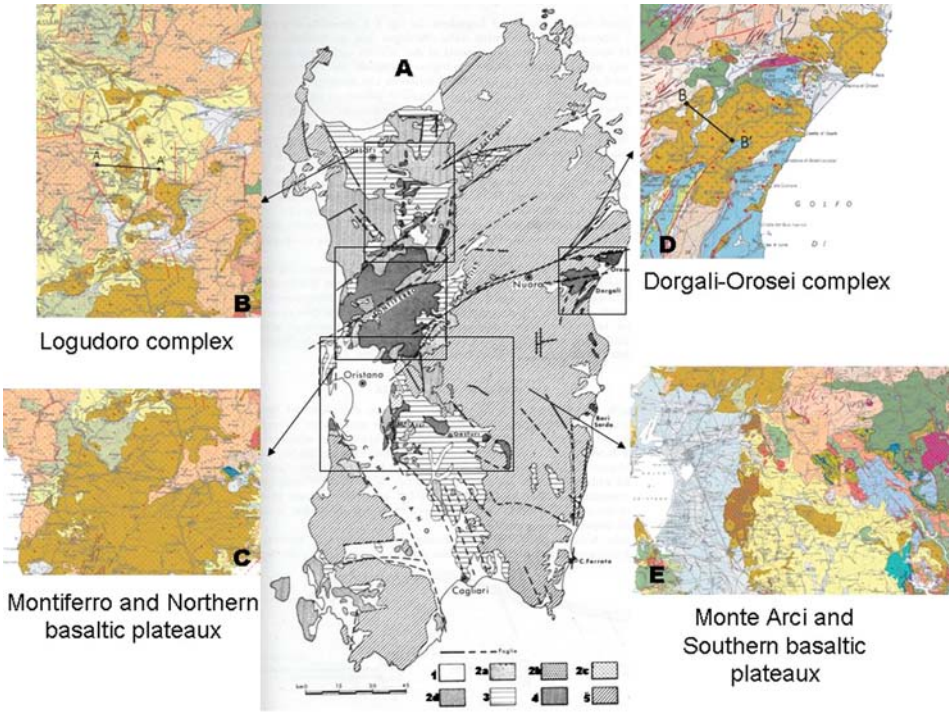

Figure 3

(A) Geological-structural-volcanological sketch of Sardinia: **unit 1)** Quaternary alluviums; **unit 2** intraplate anorogenic Plio-Quaternary activity with: **unit 2a)** Alkaline basic volcanites with alkaline affinity (3.9-Quat); **unit 2b)** Phonolite thrachyte vulcanites of Montiferro (2.8 Ma); **unit 2c**) Dacite volcanites of Monte Arci (2.9 Ma); **unit 2d)** Rhyolites (3.3-3.1 Ma) and oversaturated trachytic alkaline of Monte Arci (2.6 Ma); **unit 3)** Marine, fluvial and lacustrine sedimentary Tertiary rocks; **unit 4)** Orogenic emplacement of Oligo-Miocenic volcanites (30.11 Ma); **unit 5)** Pre-Tertiary intrusive, metamorfic and sedimentary rocks (modified by Cocozza *et al*., 1974; Beccaluva *et al*., 1975). Enlargement of four important volcanic complexes with profile traces used later in the paper (modified after Conti *et al*., 1996): B) Logudoro complex with the topographic section AA'; C) Montiferro and Northern basaltic plateau; D) Dorgali-Orosei complex with the topographic section BB'; E) Monte Arci and Southern basaltic plateau.

along the peri-Tyrrhenian margin, and the concomitant opening of the interarc Tyrrhenian Sea.

2.1. Plio-Quaternary Volcanism in Sardinia

Here we present a general view of the Plio-Quaternary deposits, and focus upon the volcanism younger than 1 Ma. In Figure 3A a geologic-structural and volcanologic sketch of Sardinia is given. The Plio-Quaternary volcanic activity produced mainly rocks from lava flows, large volcanic plateau, rarely pyroclastic flows and lava domes (Montiferro). The volcanic plateau are Orosei-Dorgali, Campeda-Planargia, and Gerrei;

the infrequent volcanic edifices are Montiferro and Monte Arci; the cinder cones are: Logudoro; very small necks are: Isola del Toro, Rio Girone, Guspini and small lava flows are Barisardo, Baunei, Capo Ferrato and Tharros (Di Battistini *et al.*, 1990; Montanini *et al.*, 1994; Lustrino *et al.*, 1996, 2002, 2004; Lustrino 1999, 2000a, 2000b, 2000c; Beccaluva *et al.*, 1985). In Figure 1A, the mentioned volcanic deposits are marked with triangles.

The absolute ages of the Plio-Quaternary volcanic deposits in Sardinia present a major problem, as many bibliographic references are found, but there is a wide disagreement between publications. We have found that in the older publications (1970 ties) the age is in better agreement (Assorgia *et al.*, 1976; Beccaluva *et al.*, 1976), whereas in more recent papers greater variability is found (Petteruti Lieberknecht *et al.*, 2003; Lustrino *et al.*, 2002, 2004; Beccaluva *et al.*, 1985). In fact, the first works referred to published radiometric ages (Savelli and Pasini, 1973; Belluomini *et al.*, 1970; Bigazzi *et al.*, 1971; Di Paola *et al.*, 1975; Savelli, 1975), while the recent works include different newer surveys. For the newer works, the radiometric ages are more precise, but differ in greater amounts between authors. Some differences may be due to problems with the radiometric age determination, linked to Argon loss in rhyolitic glass samples (Beccaluva *et al.*, 1985). Regarding our loading problem, since the timing of the loading is not known with certainty or in great detail, the analysis must be undertaken by considering the maximal and minimal expected loads that may have affected the Tyrrhenian sea-level marker.

Recent $^{40}Ar/^{39}Ar$ data (Lustrino *et al.*, 2007a) suggest that the onset of the Plio-Quaternary anorogenic magmatic phase may have occurred much earlier, in the middle Miocene ($\sim$11.8 Ma). Given the local character of the sea-level anomaly (<50 km) there is no need to include the description of all Plio-Quaternary deposits in Sardinia. Therefore, in the following, we describe only those that are relatively close to the anomaly and relatively young to be possible candidates as a source for sea-level change. A summary of the volcanic units and their respective ages is given in Table 1.

2.1.1 Logudoro. This volcanism is located between the Anglona region to the north, and the Marghine and Gocèano chains towards the southeast, in N-W Sardinia (Fig. 3B). The volcanism is similar to the other coeval volcanic deposits with fissural effusions and are mostly alkalic in character, although some transitional and subalkalic deposits also exist (Beccaluva *et al.*, 1985; 1976). This activity outcrops over an area of $\sim$500 km^2 (Lustrino *et al.*, 2004) or $\sim$300 km^2 (Beccaluva *et al.*, 1985).

2.1.2 Dorgali-Orosei and S. Pietro Baunei. The complex is located in central eastern Sardinia (Fig. 3D), near the Orosei Gulf. Its deposits ($\sim$150 km^2) overlie Paleozoic and Mesozoic substrates of limestones and dolostones, along a roughly NNE-SSW and NW-SE trending fissure system. These rocks are $\sim$80% alkaline and $\sim$20% tholeiitic lavas (Lustrino *et al.*, 2000) with alkali basalts, hawaiites, mugearites, basaltic andesites, with mantle xenoliths (Lustrino *et al.*, 2004) and unusual trace elements and isotopic ratios

(Sr, Nd, Pb), compared with other Cenozoic European volcanic rocks. This suggests a lithospheric mantle origin (LUSTRINO *et al.*, 2002).

2.1.3 Submarine volcanic activity. Twelve kilometers from Punta Nera di Osalla, north of Marina di Orosei, a submarine basaltic deposit has been found (ORRÙ, 2004). No age is available at this time.

3. Seismicity

Sardinia is considered to be a stable region, in fact the Sardo-Corso block has been stable since 7 Ma. This makes the Tyrrhenian coastline a reference level for the global sea-level change (LAMBECK *et al.*, 2004a). The stability is demonstrated by low earthquake activity, which according to the Instituto Nazionale di Geofisica e Vulcanologia (INGV) classification (INGV, 2007), belongs to the lowest grade (4) in the seismic-risk zoning of Italy. The historic macroseismic catalogue of INGV (DBMI04, 2007), contains only three events, and these have intensities less than I = 5: the first occurred in 1838 (Sant'Antioco; Lat 41°, Lon 9.25°), the second in 1924 in NW Sardinia (Lat 41.7°, Lon 8.5°) and the third in 1948 (Sardinia Sea; Lat. 40°, Lon. 8.95°). In Figure 1A the seismicity for 1971-July 2007 (NEIC, 2007) with the addition of the historic events is shown. The island is practically aseismic, except for a cluster of events in the north onshore, offshore further north and offshore to the northeast, with a maximum magnitude of M = 5.1. The position and the magnitude of the events alone cannot be responsible for the observed coastal height anomaly of the Tyrrhenian tidal notch, although some vertical movement is not impossible over 125 ky, as occurred at Capo Caccia (north Sardinia) (FERRANTI *et al.*, 2006), but again cannot explain the anomaly in Orosei Gulf where we observe a displacement of 4 m along 30 km.

4. Synthetic Load Models

In order to analyze the possible crustal response to volcanic loading and the resulting relative sea-level change along the Tyrrhenian tidal notch of Orosei Gulf, we first consider the effect of synthetic loads on the lithospheric flexure model (e.g., WATTS, 2002). The flexure $w(\vec{r})$ of the plate loaded by a topography $h(\vec{r})$ is given in the formulation in frequency-space by the equation

$$W(\vec{k}) = \frac{\rho_c}{\rho_m - \rho_c + \frac{D}{g}\left|\vec{k}\right|^4} H(\vec{k}), \tag{1}$$

where $W(\vec{k})$ is the Fourier transform (FT) of the flexure $w(\vec{r})$ of the median line of the plate, $H(\vec{k})$ is the FT of topography $h(\vec{r})$, ρ_m, ρ_c are respectively the crust and mantle densities, g is the normal gravity, $\vec{k}$ is the two-dimensional wavenumber, and D is the flexural rigidity of the plate, defined in terms of Young's modulus E, the Poisson ratio v, and the equivalent elastic thickness T_e as:

$$D = T_e^3 \cdot \frac{E}{12(1-\nu^2)}. \tag{2}$$

We calculate the flexural response to various types of loads and its dependence on the flexural parameters employed. The result is a sensitivity analysis on the vertical crustal movement in response to volcanic load, considering the variation of several parameters: elastic thickness (T_e), load radius (r), load height (H), base eccentricity (e) and distance to coast (d). The parameter space is given in Table 2, where the values used for the tests are documented. In the remainder of the paper we refer to the elastic thickness instead of to the flexural rigidity, which implies a choice of a rheologic model. We refer to standard values with E = 10^{11} Pa and $\nu = 0.25$. The elastic thickness must be scaled accordingly for a different choice of the rheologic model.

We use a load model that represents a simplified morphology of the volcanic deposits. For this, we employed a bell-shaped solid with an elliptical to circular base. The form represents a generic load, where *sig* is the square of the halfwidth (*sigt*) of the bell, *len* is the length along the bell defined by the azimuth α and *amp* is the amplitude of the bell (Fig. 4A). The load topography ($Z(x, y)$) at the point (x, y) where the load is centred at the origin ($x = 0$, $y = 0$), is given by:

$$Z(x,y) = h(x,y) \cdot amp \cdot e^{-\frac{y_r^2}{sig}}, \tag{3}$$

$$h = \left[\cos\left(\frac{x_r}{xlen}\pi\right) + 1\right]\frac{1}{2} \quad (\text{for argument of cosine} < \pi) \tag{4}$$

$$h(x,y) = 0 \quad (\text{otherwise})$$

with:

$$x_r = \cos(\alpha)x - \sin(\alpha)y, \tag{5}$$

$$y_r = \sin(\alpha)x + \cos(\alpha)y. \tag{6}$$

In Figure 4A and 4B an example load is illustrated.

Table 2

Parameters used in the synthetic load modelling. The main values are set in bold character

Name of parameter	Symbol of parameter	Values of different parameters employed by the models											Unit
base diameter	2r	0.4	1	2	3	4	5	6	7	8			km
height	H	10	60	110	160	210	260	310	360	410			m
elastic thickness	T_e	**1**	5	**10**	14	16	18	20	25	30	35	45	km
distance to coast	d	5	25	45	65	85							km
load density	ρ_c	2600	**2700**	2800	2900								kg/m^3
mantle density	ρ_m	**3300**											kg/m^3

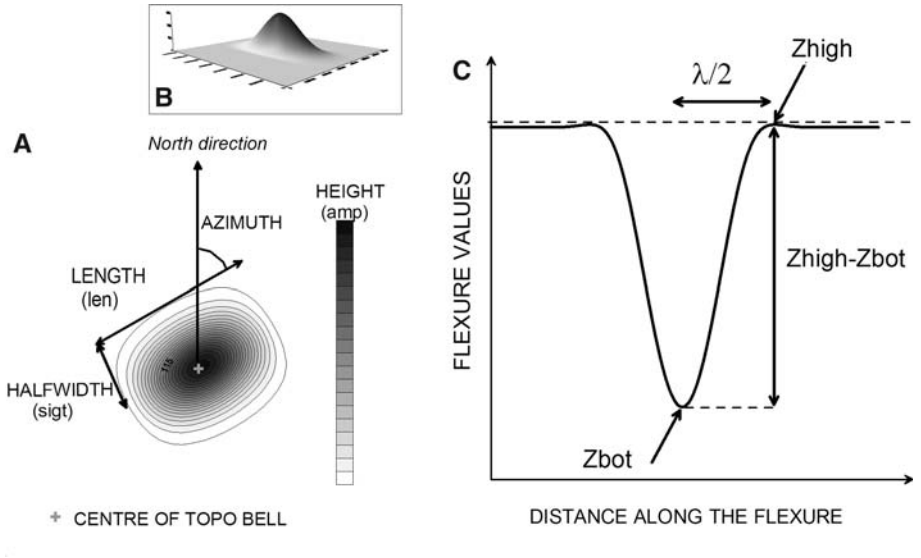

Figure 4
Cartoon illustrating the essential quantities of the synthetic loading models: A) Plane view of the synthetic load and displacement; B) Crow's view of the synthetic load; C) Essential parameters defining the flexural displacement.

4.1. Coastal Response to Synthetic Models of Variable Load Radius and Load Height

4.1.1 First case: medium flexural rigidity. In the first case we study the flexural response to a load with variable radius and height, leaving rigidity constant and allowing for several distances from the coast. The flexural rigidity has a medium value ($D = 8.9 \times 10^{21}$Nm), which corresponds to an equivalent elastic thickness of $T_e = 10$ km. The other fixed parameters are the crustal density (2700 kg/m^3), the mantle density (3300 kg/m^3), and the Poisson ratio (0.25). We consider at first a load with a circular base (radius r), and variable height (H); the values being those given in Table 2. We obtain thus for one value of T_e and a fixed distance of the load from the coast 81 load models, considering that we tested 9 different values for radius and height. We analyze the effect of the load by considering the flexure effect along a 100-km long segment of the Sardinia coastline centered on the Orosei Gulf. For each load model we extract the values of maximum (Zbot) and minimum (Zhigh) downward movement along the coastal segment; the latter possibly being transformed into an upward movement, in the case of the flexural bulge cutting the coastline. Refer to Figure 4C for an illustration of the quantities Zbot and Zhigh.

In Figure 5 we illustrate the model situation, with the single load (Fig. 5A) and the flexure displacement of the surface assuming $T_e = 10$ km (Fig. 5C) and $T_e = 1$ km (Fig. 5D). The load has a circular base of radius $r = 1.5$ km and the height $H = 200$ m.

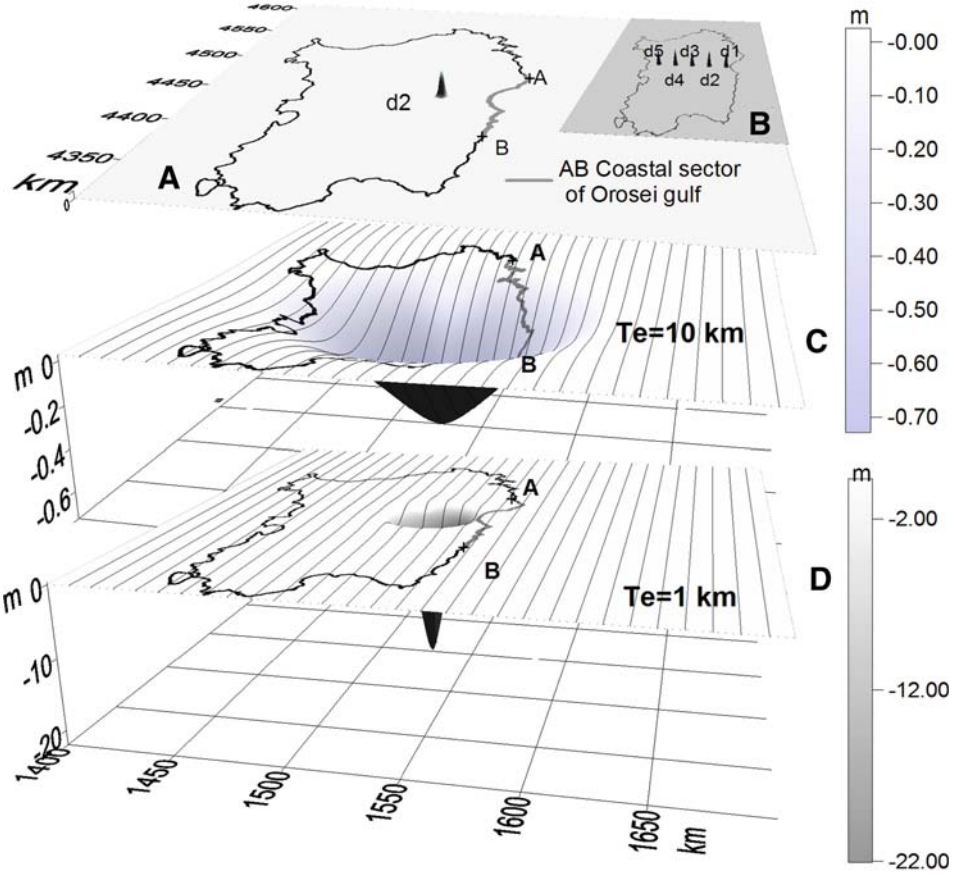

Figure 5

Cartoon illustrating the different model conditions of the synthetic loading: A) View of single load (d2) and B) load placed at a series of distances from the coast; C) Flexural displacement in response to single load, $T_e = 10$ km; D) As case C but for $T_e = 1$ km. Small crosses named A and B show initial and end point of coast profile Dorgali-Orosei.

These values are synthesized with bidimensional diagrams (abscissa: height, ordinate: radius), in which all the other parameters on which the flexure depends are kept constant (Fig. 6). We interpolate the calculated values on a regular grid, using a fourth-order polynomial surface. We show 5 cases in which the load to coast distance varies from 5 km to 85 km, in steps of 20 km. As expected, the flexure increases with increasing load mass, attaining greatest values for the maximum load corresponding to $H = 410$ m, $2r = 8$ km.

Incrementing the distance between the load and the coast by steps of 20 km, the flexural values decrease by 30%, 50%, 60% and 90% with respect to the starting value at 5-km distance from the coast, respectively. The models show that a load set at distance

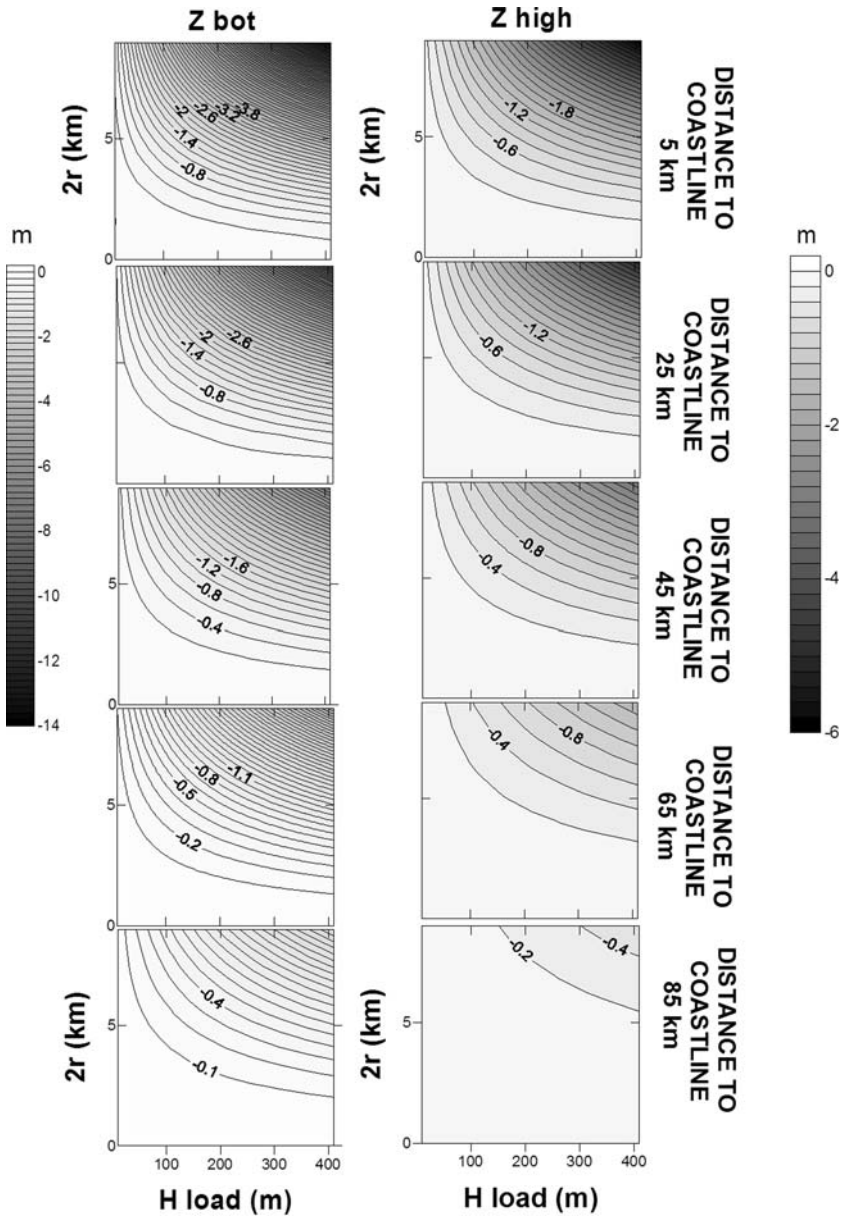

Figure 6
Crustal flexure along a coastline due to a synthetic load: flexural response due to a load with varying radius and load height; flexural rigidity constant ($T_e = 10$ km), different coastal distances.

85 km has a non-negligible effect on the coastline: taking for instance the model with $H = 410$ m, $2r = 8$ km and $d5 = 85$ km, the flexure attains the values -1.5 m and -0.4 m, respectively.

Due to the fact that the load increases with the square of the base radius, the flexure depends strongly on this value. For all considered heights and distances (5 to 85 km) to the coast, the value $2r < 2-3$ km corresponds to very small flexural amplitude (maximum flexure isoline: 20 cm), while if $2r = 4$–6 km an observable flexure is obtained (up to a few meters).

Considering a constant load height (410 m), a radius decrement (3.5, 3, 2.5, 2, 1.5, 1, 0.5, 0.2 km) corresponds to the percentage reductions with respect to the radius (r) = 4 km of 79%, 58%, 40%, 26%, 15%, 6%, 2% and 1%, respectively. An increase of height with constant radius produces a proportional flexural increase.

The amount of flexure, along the coastal segment for varying r and H at the 5 distances, is reduced with the increasing load-to-coast distance ($d2 = 25$ km, $d3 = 45$ km, $d4 = 65$ km, $d5 = 85$ km) to a value which is 85%, 53%, 25% and 8% of the maximum value for $d1 = 5$ km. We can see that the effect of the load in all these cases is the same: a downward flexure along the coast.

4.1.2 Second case: Low flexural rigidity. One important scaling parameter is the flexural rigidity or equivalently the elastic thickness, that controls the flexural response. In the following we take the radius, height and distance as above, using a low value of flexural rigidity $D = 8.9 \cdot 10^{18}$ N m, (which corresponds to $T_e = 1$ km). The flexure along the eastern coastline for the different cases is shown in Figure 7. In Table 3 the extreme values of the flexure along the coastline are given. The maximum downward deflection is 20-fold for the load nearest the coast, with respect to the previous case ($D = 8.9 \cdot 10^{21}$ N m, $T_e = 10$ km). As the involved wavelengths are smaller, the flexural bulge is seen along the coastline in the form of an uplift (4 m), for the load close to the coast. The flexural response decreases quickly for a load more distant to the coast, and Zbot at 25 km is only $\sim 18\%$ of the value for the load placed at 5 km distance to coast, while the Zhigh is similar: 4.3 m for $d1 = 5$ km, and 4.25 m for $d2 = 25$ km. For $T_e = 10$ km we did not observe the bulge along the coastline profile, because it is located at a greater distance from the load. It is interesting to observe that for $T_e = 1$ km the maximum bulge is close to the load (~ 17 km) with a maximum amplitude (Zhigh) of 4.3 m and that it is apparent up to a distance of about 60 km; in fact, the positive values decrease in amplitude and arrive to zero for $d > 65$ km, while for $T_e = 10$ km the positive values are found at about 125 km.

4.2. Coastal Response for Synthetic Models of Variable Load Radius and Load Position

In this model we considered the flexural response for the variation of radius (r) and the load position (d), where the values vary as given in Table 2. The elastic thickness is constant ($T_e = 10$ km) and the load has constant height (200 m), the remaining parameters having values as in Section 4.1 The variation of flexure is studied along the coastal sector of the Orosei Gulf. This model is similar to the preceding one, and we

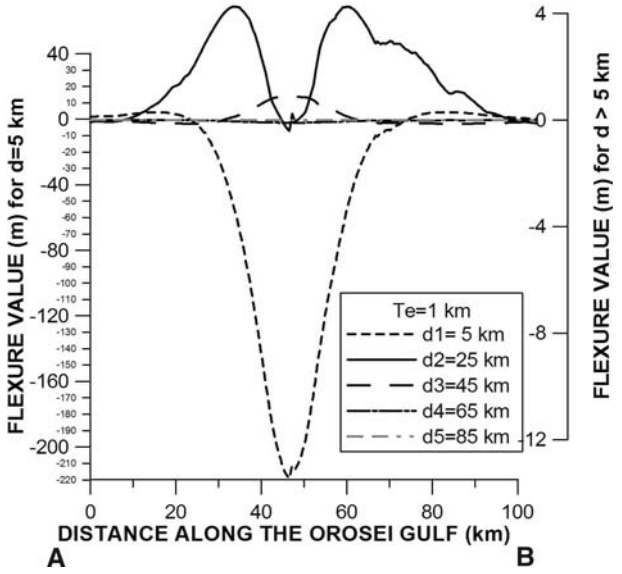

Figure 7

Flexural displacement along the coast profile Dorgali Orosei for a load placed at different distances d1,…,d5 from the coast. Left abscissa for distance value d1, right abscissa for distance values d2,…,d5. The load has a circular base of radius r = 4 km, height h = 410 m. Only for this case of an elastic thickness with an unrealistically low value, the uplift of the coastline can be produced.

Table 3

Flexure due to a synthetic load of height H = 410 m and radius r = 4 km set at different distances from the coast (5, 25, 45, 65 and 85 km) with T_e = 1 km: The value for Zbot, Zhigh and Zhigh-Zbot and the respective percentage value with respect to the nearest case with distance to coast = 5 km are reported

	Zbot	*%decr.*	*Zhigh*	*%decr.*	*Zhigh-Zbot*
D1 = 5 km	−219	100%	4.3	100%	223.5
D2 = 25 km	−0.41	18%	4.25	98%	4.66
D3 = 45 km	−0.14	6%	0.92	22%	1.06
D4 = 65 km	−0.1004	4%	0.005	11%	0.1054
D5 = 85 km	0	0%	0	0%	0

obtain the value of Zbot, Zhigh along the sector analyzed for the different 81 load models.

The values are again interpolated on a regular grid with a fourth-order polynomial surface. Figure 8 shows the values of Zbot and Zhigh for the range of radius and positions. The flexure is always downwards and no positive values are present. The values of Zbot depend strongly on the radius of the load, and also on the distance to the coast. The difference between Zbot and Zhigh is small, and this is linked to the great wavelength that characterizes the flexure (see Fig. 5C).

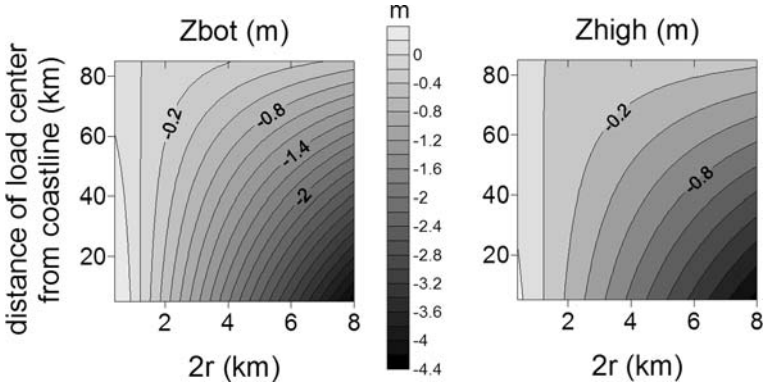

Figure 8
Extreme flexure values (Zbot, Zhigh) along the coast segment for a synthetic load model for varying coastal distance (d) and load radius (r). The elastic thickness is constant (10 km) and the load has the constant height (200 m).

4.3. *Effect of the Variation of Elastic Thickness on the Coastal Response*

We now investigate the variation of flexure in function of elastic thickness. The elastic thickness is an important parameter to describe the flexure. The parameters employed are $H = 200$ m, $r = 4$ km and T_e variable with the values given in Table 2.

We illustrate the flexural response along a profile that has different lengths according to the T_e value (Fig. 9A). For $T_e = 10-40$ km, the profile is 600-km long, while for $T_e = 1-5$ km it is 300 km. The flexure is described by Zbot (corresponding to the central point of load's application), Zhigh and Zhigh-Zbot.

We analyzed the pattern of Zbot, Zhigh and Zhigh-Zbot and found a rapid decrease in the flexural values for each increment in T_e (Figs. 9B, C, D). Moreover we can see how the flexural sag broadens with an increase of T_e, while the excursion of the bulge (Zhigh) decreases (Fig. 9E). Also the distance of the maximum bulge uplift changes: for $T_e = 40$ km, Xbulge is at 490 km from the application load, while for $T_e = 1$ km Xbulge is found at only about 30 km distance.

4.4. *Influence of the Load's Base Geometry*

We now examine to what extent the flexure is sensitive to the variation of the geometry of the load's base. Purposeful to this, we vary the eccentricity of the load. We adjust the major *(a)* and minor axes *(b)* so that the total area is constant (250 km^2), and employ the following eccentricities (e) = 0, 0.2, 0.4, 0.6, 0.8.

In order to retrieve the half axis values of ellipse and the radius of a circle of the same area, we employed the formulas

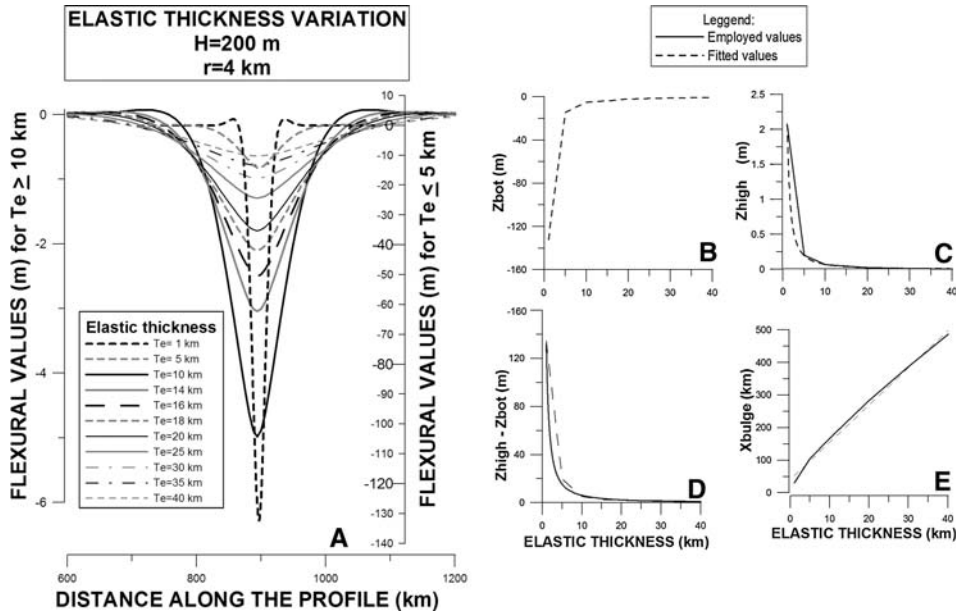

Figure 9

Flexural response for different values of the elastic thickness for a simple model of H = 200 m and r = 4 km, and T_e = 1-40 km of elastic thickness. In (A) pattern of flexure along a centred profile; (B) Zbot in function of T_e; (C) Zhigh in function of T_e; (D) Zhigh-Zbot in function of T_e; (E) Radial distance from source (Xbulge) of the maximal bulge for different values of T_e.

$$A_{\text{ellipse}} = a \cdot b \cdot \pi, \tag{7}$$

$$e = \sqrt{1 - (b^2/a^2)}. \tag{8}$$

We find that there is little variation of flexure for a variation of eccentricities (Fig. 10). Therefore the flexure is clearly linked to the development of the load area and not to the geometry of the mass.

5. *Volcanic Load Models Applied to Sardinia*

At this point we study the effect that the volcanic loads have on displacement along the coast of Sardinia, in order to explain the height-anomaly of the Tyrrhenian notch observed in the Orosei Gulf. For this purpose, we consider both surface volcanic loads as well as the effect of a possible magmatic intrusion, with age presumably younger than 1 Ma.

In order to estimate the volume of the loads, we overlay the geologic map on a digital terrain model and estimate the thickness of the volcanic layer where the layer is cut by the erosional effect of rivers. We use the SRTM (Shuttle Radar Topography Mission) digital

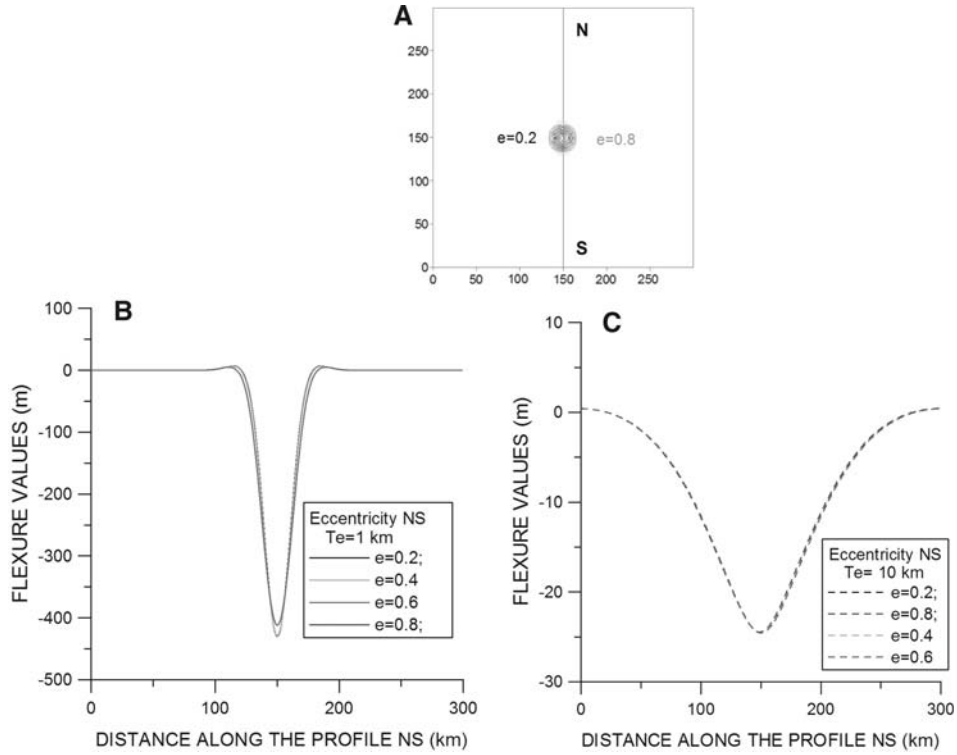

Figure 10

Flexural displacement along a profile centered on the load. Load has elliptical base with variable eccentricity and constant area. The effect of eccentricity is very small for low T_e-values (e.g., $T_e = 1$ km), and negligible for higher T_e (e.g., $T_e = 10$ km).

elevation model (Farr *et al.*, 2007) with a 3 arc-sec spatial resolution. As the geological maps are given in digital form and are georeferenced, the superposition with the SRTM model should have the same precision as the geological map. The thickness estimate will be more correct, the less the volcanic layer has lateral thickness variations. We model the loads in the form of a solid similar to a shield, with an elliptical base. The model parameters are the flexural rigidity or equivalently the effective elastic thickness (T_e), the load density and the mantle density. The latter are set to the values $\rho_c = 2700$ kg/m^3 and $\rho_m = 3300$ kg/m^3, respectively. For the elastic thickness we calculate the flexure for different values of flexural rigidity, assuming values of $D = 8.9{\cdot}10^{21}$, $7.1{\cdot}10^{22}$, $2.4{\cdot}10^{23}$, $5.6{\cdot}10^{23}$ and $11.1{\cdot}10^{23}$ N m (corresponding to elastic thicknesses $T_e = 10$, 20, 30, 40 and 50 km).

5.1. Dorgali-Orosei Load Model

The first load we consider is the Dorgali-Orosei complex (Fig. 3D), which is very near the anomalous coastline. The ages given for this unit are between 4 Ma and 2 Ma

(Beccaluva *et al*., 1985; Petteruti Lieberknecht *et al*., 2003; Lustrino *et al*., 2004). The basalts belong to the Plio-Pleistocene succession (unit 5b of Conti *et. al*., 1996), the age of which is defined between 0.14 to 5 Ma. There is some morphological evidence that the basalts could be as recent as a few 100 ka due to the freshness of basalt flows and the position of the basalts relative to the notch, so we include them into our loading study. In Figure 11A we show the topography along the profile B-B' (see Fig. 3D). The outcropping basalts are marked by the symbols bas1 and bas2. The thickness of the basalts is approximated by the height H. The Cedrino River is seen to cut the basalts, allowing the estimate of the minimum thickness. The basalts are covered by Quaternary deposits.

The load is defined by the greater (a) and minor axis (b) of the elliptical base, the azimuth of the major axis and the height. The load is composed of two units, the northern load model (model A) and the southern model B (Fig. 11B), the details of which are found in Table 4.

The flexure due to the Cedrino volcanic load along the entire coastline of Sardinia is divided into the western (Fig. 11C) and eastern segment (Fig. 11D). The short-wavelength variations of flexure along the profile are due to the varying distance of the coastline from the load.

Along the western coastline (Fig. 11C) we find that the flexure reaches positive values (up to 16 cm) for $T_e = 10$ km along some parts of the coast (between Cagliari Gulf and south of Oristano Gulf; between Alghero Gulf and Asinara Gulf) due to the fact that the coastline intersects the flexural bulge. For greater elastic thickness the values are only negative. For the eastern coastline (Fig. 11D), we find that the flexure has only negative values for all rigidities tested. An increase of the flexural rigidity leads to a decrease of the flexure amplitude and to an increase in the characteristic wavelength. The maximal downward flexure is found near the center of the Orosei Gulf, which is close to the load application and amounts to -4.5 m for the rigidity value of $T_e = 10$ km. For higher values of rigidity the maximum downward flexure amounts to 33% of this maximal deflection for $T_e = 20$ km, 17.7% for $T_e = 30$ km, 14.8% for $T_e = 40$ km and 13.3% for $T_e = 50$ km.

The conclusion is that the basaltic volcanic load of Orosei-Dorgali does not explain the positive anomaly of Orosei Gulf.

5.2. *Logudoro Load Model*

The second load that we consider is the Logudoro volcanic complex, as different references discuss relatively recent activity, as late as 0.11 Ma (Petteruti Lieberknecht *et al*., 2003 and Lustrino *et al*., 2004). We follow the procedure explained above to estimate the volume of the loads, and in Figure 12A one section across the complex is shown (the profile position is shown in Fig 3B). Again bas 1 and bas 2 define the outcrops of the basalts and H the estimated basalt thickness. The Plio-Quaternary volcanic deposits cover the Oligo-Miocene volcanic load with fissural events (units 11, 12 in geologic map

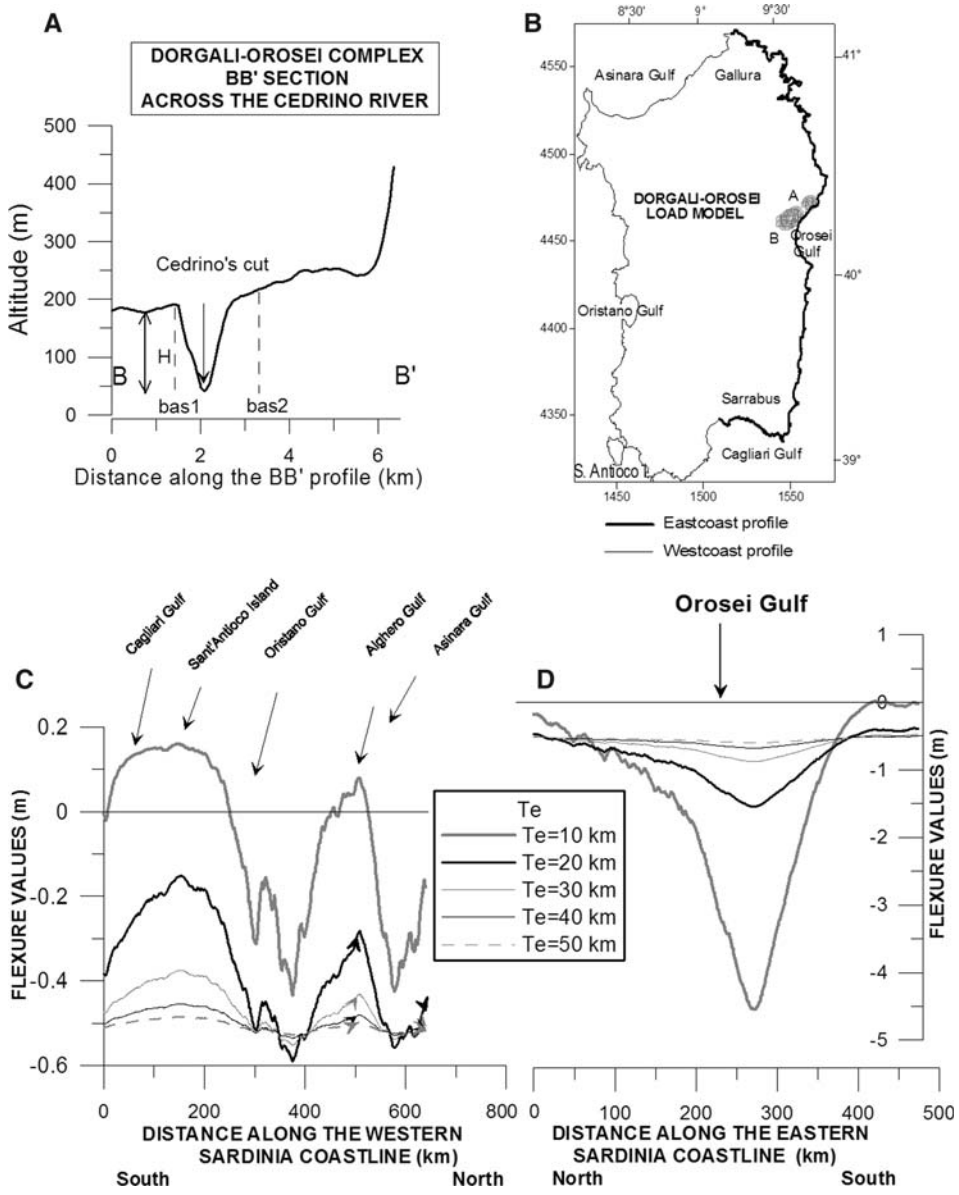

Figure 11

Dorgali-Orosei volcanic load. A) Section across the topography used to estimate the basalt thickness: the basalt outcrop along the profile extends between positions bas1 and bas2, Dorgali-Orosei topographic section BB', the location of the profile is shown in Figure 3D; B) Load model Dorgali-Orosei: black: eastern coastal segment; grey: western coastal segment; C) flexure along the western coastal segment for different T_e-values; D) flexure along the eastern coastal segment for different T_e-values.

Table 4

Details of the Dorgali-Orosei load model, composed of two deposits, A and B (see Fig. 11B): Geographical coordinate of the centre of elliptical base, the greater (a) and minor axis (b), the height of the load (H) and the azimuth of the major axis

Model	Latitude	Longitude	High	Azimuth	Axis a	Axis b
A	40.41°	9.73°	100 m	165°	5.5 km	5 km
B	40.32°	9.6°	130 m	150°	12 km	10 km

Conti *et al*., 1996), and cover the younger continental and marine units of the Ussana Formation (units 10c in geologic map, Conti *et al*., 1996) and Citerri Formation (units 10a, Conti et al., 1996). We have modelled the volcanic complex as a composite of six distinct bodies (A-F, Fig. 12B), defined by the position of the center, the maximal height, the azimuth of the major axis, and the minor and major axes of the elliptical base (Table 5).

Again we display the crustal flexure for different values of flexural rigidity, along the western and eastern Sardinia coastal segments (Fig. 12). The western profile (Fig. 12C) shows very well the flexural response to the load which creates an important downward flexure for all T_e values. The maximum downward flexure is found between the Oristano Gulf and the Asinara Gulf (km 270-690 of the profile) due to the nearness of the load.

We find that the bulge is cut by the coast along the first 200 km of the profile for low elastic thickness ($T_e = 10$ km), with a maximum bulge height of 3.3 cm. It is not present with higher values of elastic thickness. Along the eastern profile (Fig. 12D) the flexure is again positive only for low T_e ($T_e = 10$ km), and the maximum upward movement is 6 cm. It occurs along the southernmost 100 km of the profile, that is in the southeastern sector of the Sardinia coastline and in the eastern Cagliari Gulf. Along the northern 400 km of the profile the flexure is downward for all values of T_e employed.

Also in this case we find that the load model does not explain the anomaly values discovered along the Orosei Gulf: in fact the Gulf is located at 250–300 km from the starting point of the eastern sector of Sardinia coastline where the flexure is negative for all values of T_e tested.

5.3. Mogi Model and Laccolith Model

In the previous paragraphs we showed that the surface volcanic loads are unable to explain the positive anomaly of the notch height. We therefore proceed to consider the crustal deformation due to a magmatic intrusion. We consider two models: A spherical pressure source in the crust (Mogi, 1958) and a model which geologically simulates a laccolith. The laccolith is an igneous intrusion in the form of a lens-shaped body, with the characteristic of greater lateral than vertical dimensions. The laccolith is formed by magma that has been injected between planes of flat rock layers at a pressure that is sufficiently great to force the overlying strata upward leading to a domelike shape with a

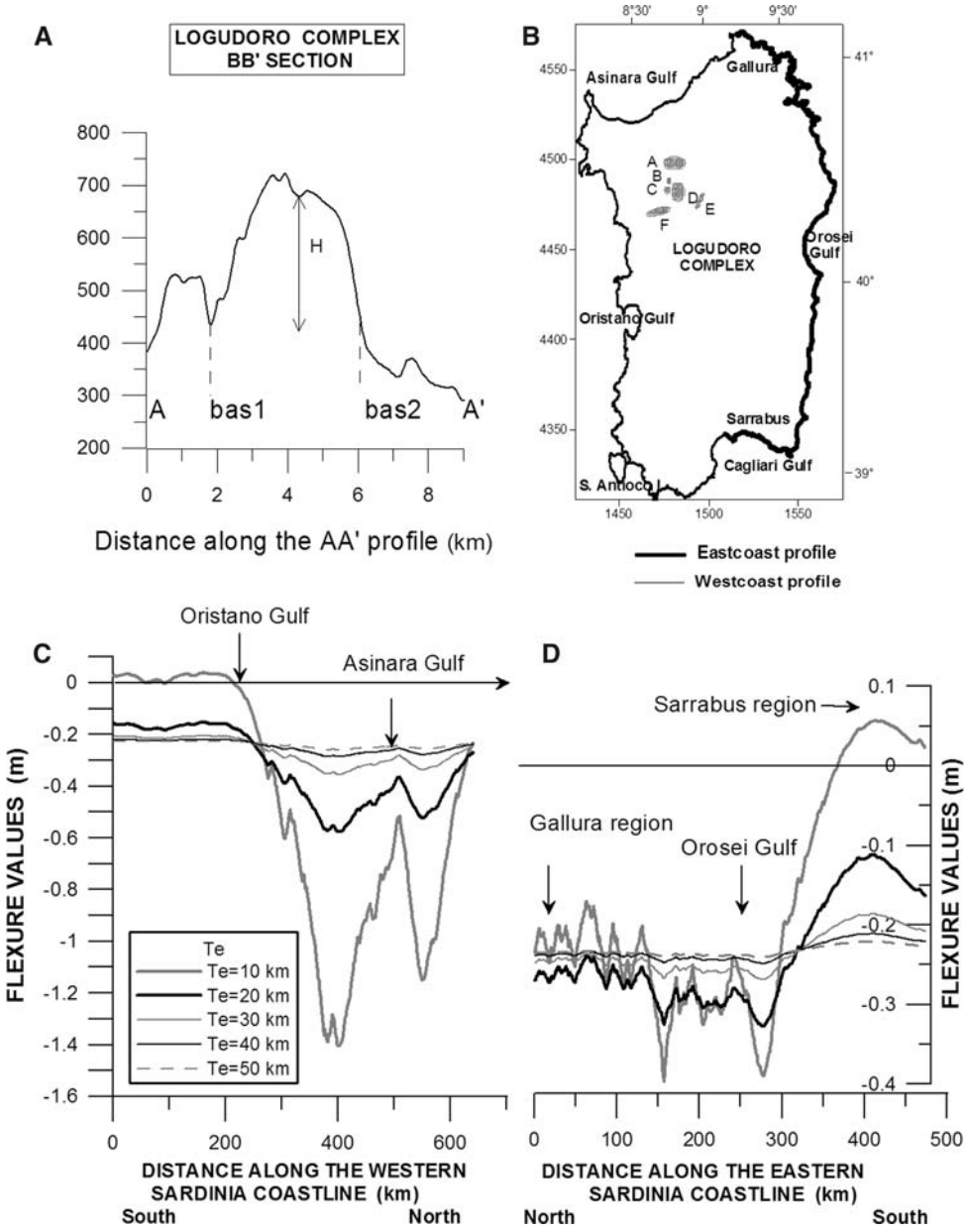

Figure 12

Logudoro volcanic load. A) Section across the topography used to estimate the basalt thickness: the basalt outcrop along the profile extends between positions bas1 and bas2, Logudoro topographic section of the profile is shown in Figure. 3B; B) Load model Logudoro; black: eastern coastal segment, grey: western coastal segment; C) flexure along the western coastal segment for different T_e-values; D) flexure along the eastern coastal segment for different T_e-values.

Table 5

Details of the Logudoro load model, composed of deposits A-F: Geographical coordinate of the centre of elliptical base, the greater (a) and minor axis (b), the height of the load (H) and the azimuth of the major axis

Model	Latitude	Longitude	High	Azimuth	Axis a	Axis b
A	40.64°	8.8°	50 m	0°	7 km	4 km
B	40.55°	8.75°	240 m	0°	2 km	1 km
C	40.50°	8.75°	200 m	0°	2 km	1.5 km
D	40.50°	8.82°	30 m	0°	6 km	4 km
E	40.46°	8.9°	70 m	117°	6 km	1 km
F	40.4°	8.69°	100 m	105°	8 km	2 km

planar base. We extend the two-dimensional laccolith model of TURCOTTE and SCHUBERT, (2002) to the axis-symmetrical case by using the mathematical expression for the deformation of an elastic plate deformed by a cylindrical source (LOVE, 1944; TIMOSHENKO and WOINOWSKY-KRIEGER, 1959).

5.3.1 Mogi model. One model frequently used to predict the deformation tied to volcanic activity is the Mogi model (MOGI, 1958). It considers a spherical overpressure at a fixed depth in a half space. The equation describing the vertical deformation $W(x, y, z)$ at the point defined by the coordinates (x, y, z; z positive upwards) is the following (MOGI, 1958),

$$W(x,y,z) = \frac{a_m^3 P}{4\mu} \frac{1}{\left\{(z+2d)^2+R^2\right\}^{5/2}} \left(7z^3 + 38dz^2 + 68dz^2 + 40d^2 + 4dR^2 + zR^2\right) + \frac{a_m^3 P}{4\mu} \left[\frac{R}{(z^2+R^2)^{3/2}} + \frac{z+2d}{\left\{(z+2d)^2+R^2\right\}^{3/2}}\right], \tag{9}$$

where a_m is the radius of the sphere affected from the hydrostatic pressure, P is the change in hydrostatic pressure in the sphere, d is the depth of the center of the sphere from the surface, R^2 is $R^2 = x^2 + y^2$ and μ is the Lame's constant. In our case, the vertical deformation is evaluated at the surface, so we put $z = -d$.

We have tested the Mogi solutions for different models. The used parameters are described in Table 6. The point of load application and the pressure are kept constant. For the value of the pressure we adopt the order of magnitude proposed by FERNÁNDEZ and RUNDLE (1994), which is $P = 0.25$ GPa. We analyze the vertical displacement along a linear profile centered on the source, as shown in Figure 13.

In general we observe that for a constant radius, the flexure wavelength in the Mogi model increases with depth, whereas the maximum height of the vertical displacement decreases. A decrease in rigidity (μ) is accompanied by smaller flexure wavelength and greater displacement-amplitude.

Table 6

Parameters employed for the synthetic Mogi model-situations: the source is described by the depth to the intracrustal sphere (d), the radius of the sphere (r_m) and the rigidity (μ). The pressure (P) is set to the value 0.25 GPa

Radius r_m	Depth d	Lame's constant μ
1 km	5 km	$0.23 \cdot 10^{11}$(Pa)
1 km	10 km	$0.23 \cdot 10^{11}$(Pa)
1 km	15 km	$0.23 \cdot 10^{11}$(Pa)
1 km	5 km	$0.21 \cdot 10^{11}$(Pa)
1 km	5 km	$0.19 \cdot 10^{11}$(Pa)
1 km	10 km	$0.23 \cdot 10^{11}$(Pa)
1.5 km	10 km	$0.23 \cdot 10^{11}$(Pa)
2 km	10 km	$0.23 \cdot 10^{11}$(Pa)

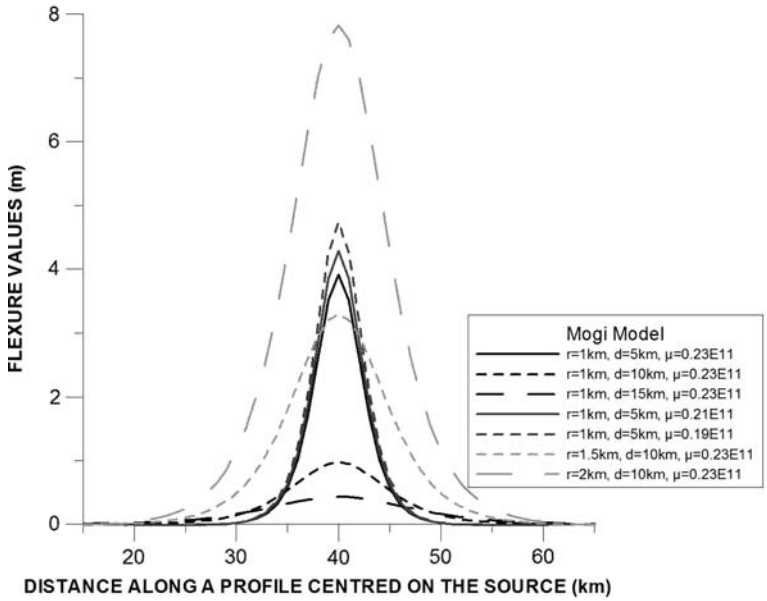

Figure 13

Flexure due to the synthetic Mogi model for different values of depth of intracrustal sphere (d), the radius of the sphere (r), and the crustal rigidity (μ). The pressure is constant and assumed $P = 0.25$ GPa. The black lines are for models with constant μ and r (respectively 0.23–10^{11} Pa and 1 km), and d from 5 to 10 km; the dark grey lines are for models with constant r and d (respectively 1 km and 5 km) and μ from 0.21–10^{11} to 0.19–10^{11} Pa; the grey lines are for models with constant d and μ (respectively 10 km and 0.23 10^{11} Pa) and r from 1.5 to 2 km.

The profiles shown in Figure 13 can be summarized as follows: for $r = 1$ km and increasing depth ($d = 5$, 10 and 15 km), the wavelength of flexure increases and the maximum resulting vertical displacement is 3.9, 0.97 and 0.43 m, respectively; for depth $d = 10$ km and $r = 1$, 1.5, and 2 km, the maximum displacement reaches respectively

0.97, 3.28 and 7.8 m; with $r = 1$ and $d = 5$ km with varying rigidity μ (0.23, 0.21 and $0.19{\cdot}10^{11}$ Pa) there is little variation in displacement-amplitude, of the order of 0.8 m between extremes. Regarding the application of the models to the Orosei Gulf, due to the fact that the contour lines that cut the coast must decrease from north to south, the application point of the force in the Mogi model must be applied to the north of the Orosei Gulf to explain the MIS 5.5 notch anomaly. We find that a single Mogi-source, with acceptable source parameters (depth range of $d = 23$–26 km, radius between $r = 2.6$–3.4 km, $\mu = 0.19$–$0.23{\cdot}10^{11}$ Pa) cannot describe the anomaly because the flexure wavelength is smaller than necessary. The depth limitation is due to the fact that the crust is 20–25 km thick (Scrocca *et al.*, 2003; Nicolich, 2001; Nicolich and Dal Piaz, 1992; Panza *et al.*, 2007), which poses an upper limit to the depth of the source.

5.3.2 Laccolith model. The Laccolith model assumes a cylindrical source, in which the pressure source (P) is distributed over a circular area of radius (b). This circular area of radius b corresponds to the top of the magma conduct. We define the flexure $w(r)$ (r denotes the distance of the calculation point from the center of the plate) of a circular plate of radius a and of thickness h, supported along the edge by the equations given by Timoshenko and Woinowsky-Krieger (1959):

$$w(r) = \frac{W}{16\pi D}\left\{\frac{3+\sigma}{1+\sigma}\left(a^2 - r^2\right) + 2r^2 \log\frac{r}{a} + b^2\left[\log\frac{r}{a} - \frac{1-\sigma}{2(1+\sigma)}\frac{a^2 - r^2}{a^2}\right]\right\} \quad r \le a$$

$$w(r) = \frac{W}{16\pi D}\left[\frac{3+\sigma}{1+\sigma}a^2 + b^2 \log\frac{b}{a} - \frac{7+3\sigma}{4(1+\sigma)}b^2\right] \quad r = 0 \tag{10}$$

where $W = (P - \rho g h)\pi b^2$, with $\rho = 2700$ kg/m^3, σ is the Poisson ratio, for which we use the standard value of 0.25, and the flexural rigidity is $D = 1.1{\cdot}10^{19}$ N m, corresponding to a plate thickness of 5 km. The plate supported at its edge has zero deflection along the edge. A sketch of the model is found in Figure 14A.

The flexure for a disk clamped at its edges is very similar, with the difference that the flexure is of smaller amplitude for the same applied pressure. A clamped plate has both deflection and slope of deflection equal to zero along the edge (Timoschenko and Woinowsky-Krieger, 1959).

We have explored the parameter space that defines the model and compared the resulting updoming with the observations. The fact that the anomaly decreases southwards along the coast constrains the position of the source to northwards of the highest point of the anomaly. For the value of the pressure, as in the previous case, we refer to the value proposed by Fernández and Rundle (1994), (P = 0.25 GPa), and vary the values between P = 0.2 and 0.3 GPa. The plate radius is allowed to vary between 10 and 100 km and the source radius between 0 (point source) and 1 km. We find that the observations are reproduced with values of $a = 40$–50 km, $b = 0.32$–0.37 km, $P = 0.27$–0.28 GPa for different positions of the source application (Table 7). The model curves obtained for the different cases reported in Table 7 are outlined in Figure 14A.

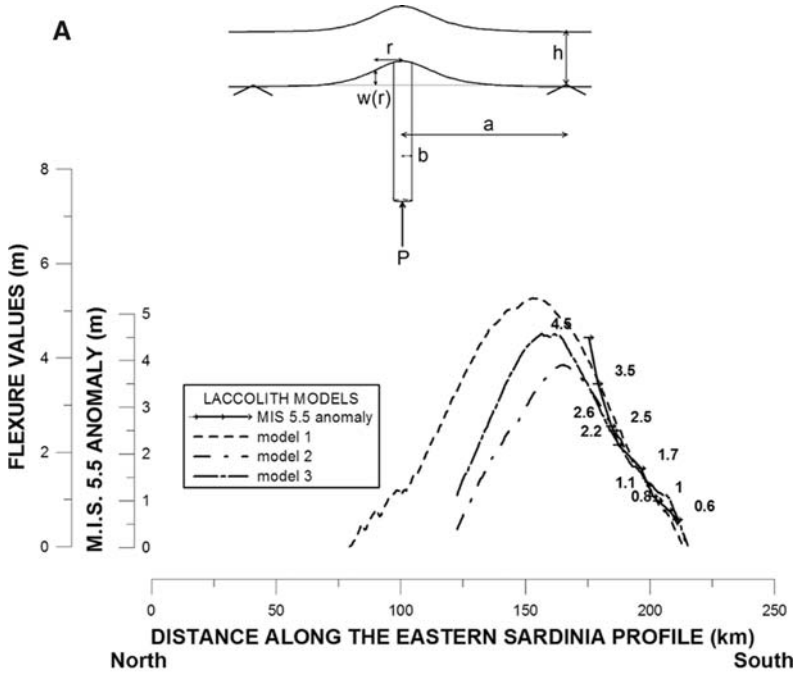
A
r
h
w(r)
a
b
P
FLEXURE VALUES (m)
M.I.S. 5.5 ANOMALY (m)
LACCOLITH MODELS
MIS 5.5 anomaly
model 1
model 2
model 3
4.5
3.5
2.6
2.2
2.5
1.7
1.1
0.8
1
0.6
DISTANCE ALONG THE EASTERN SARDINIA PROFILE (km)
North
South

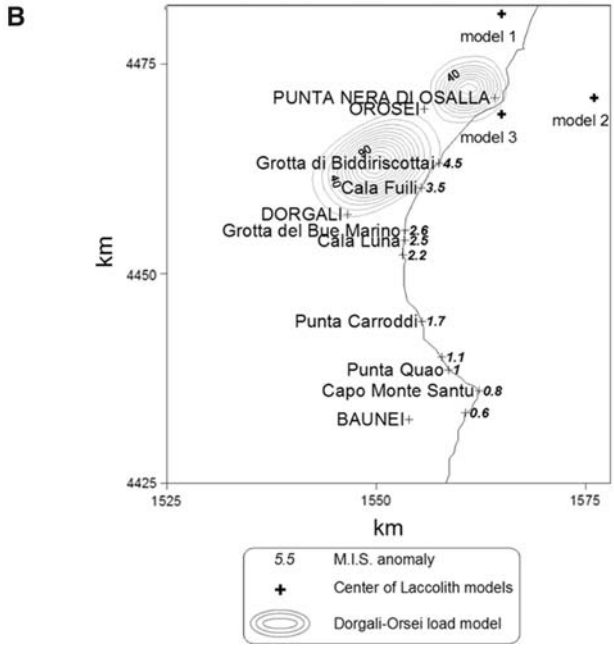
B
model 1
model 2
model 3
PUNTA NERA DI OSALLA
OROSEI
Grotta di Biddiriscottai
Cala Fuili
DORGALI
Grotta del Bue Marino
Cala Luna
Punta Carroddi
Punta Quao
Capo Monte Santu
BAUNEI
4.5
3.5
2.6
2.5
2.2
1.7
1.1
1
0.8
0.6
km
km
5.5 M.I.S. anomaly
Center of Laccolith models
Dorgali-Orsei load model

◀ Figure 14
A) Plot of upward deformation due to the laccolith model for different points of application and sketch of laccolith model; for the parameters of the model see equation (10). B) Geographic location of the models along the Orosei Gulf. The black numbers along the coast are the height of anomaly MIS 5.5 (Ferranti *et al*., 2006) and the neighboring towns are written to the left in small letters, the capital letters are for the main towns; the small black crosses indicate the center of the load application of the laccolith models; the grey ellipses show the Dorgali-Orosei load model (Fig. 11B).

Table 7

Parameters describing the laccolith model for different points of application of the upward oriented force. Easting, Northing: Geographical position in Gauss Boaga coordinates of force application point; A: plate radius; B: dyke radius; P: pressure in GPa. The models have a constant crustal and mantle density respectively of 2800 kg/m^3 and 3300 kg/m^3

	Different point-application points			
	Model 1	Model 2	Model 3	Unit
Easting (km)	1565	1576	1565	km
Northing (km)	4481	4471	4469	km
a (km)	50	44	40	km
b (km)	0.32	0.37	0.34	km
P (GPa)	0.28	0.27	0.28	GPa

Here we have subtracted the expected value (7 ± 2 m) from the observed height of the notch so as to obtain the height anomaly. We find that the height anomaly can be explained satisfactorily by the model, although the model parameters are not unambiguously determined. We obtain the best agreement when the source is positioned at latitude between 40.38°N and 40.48°N, and at a longitude between 9.76°E and 9.89°E leading to an uncertainty of 11 km. The range of possible positions is marked by the crosses shown in Figure 14B.

6. Discussion

In this work we explain the Tyrrhenian notch tilting (Antonioli *et al*., 1999) along the Orosei Gulf (NE Sardinia) as being due to a magmatic intrusion that must have occurred either after the notch was formed, or shortly before. In the past (Bigi *et al*., 1992), the notch inclination had been explained qualitatively by the association of the tilting with the residual activity in the nearby Pliocene-Quaternary Cedrino Volcanic field (for this paper, the Dorgali-Orosei complex), whose activity ended at 140 ka, shortly before the MIS 5.5.The fact that the tilting of the notch anomaly is absent at a greater distance (Antonioli *et al*., 1999; Antonioli and Trainito, 2005) is an indication of the local character of the anomaly.

In order to investigate the influence of volcanic loads on the vertical movement of the coast, we used the isostatic regional flexure model (Watts, 2002). When seeking a candidate that could have provoked the notch anomaly by loading, we must consider volcanic deposits that are younger or not substantially older than the age of formation of the notch. This is because for old loads, the crust would have already reached its deformed equilibrium at the time of formation of the notch, hence the notch itself would be horizontal and undeformed.

A review of the relevant literature (Beccaluva *et al.*, 1975; 1985; Petteruti Lieberknecht *et al.*, 2003; Lustrino *et al.*, 2004; 2007b; Conti *et al.*, 1996) has shown that there are relevant differences in the published ages for every volcanic deposit.

Another problem is due to the fact that authors do not determine the ages for individual volcanic complexes, but rather give generic ages that apply to several volcanic deposits. For some authors (Beccaluva *et al.*, 1985; Petteruti Lieberknecht *et al.*, 2003; Lustrino *et al.*, 2004) the final activity for the Dorgali-Orosei complex is over 1-2 Ma old; for Beccaluva *et al.* (1975) and Conti *et al.* (1996), the final limit is extended into the Quaternary. The geological map of Sardinia (Conti *et al.*, 1996) included the fissural emissions of the last volcanic activity, and the succession of basaltic lava flows could have complicated the temporal distinction of the samples.

The only volcanic deposit which according to the existing literature is of relatively young age is the Logudoro complex. In fact, the activity of the Logudoro complex ended 0.15 Ma according to Beccaluva *et al.* (1985), 0.11 Ma according to Petteruti Lieberknecht *et al.* (2003), 0.1 Ma according to Lustrino *et al.* (2004) and 0.4 Ma according to Lustrino *et al.* (2007b). According to some authors the final activity for the Dorgali-Orosei complex is older than 1 Ma (Beccaluva *et al.*, 1975; 1985; Petteruti Lieberknecht *et al.*, 2003; Lustrino *et al.*, 2004; 2007b), and thus could not be considered responsible for the notch anomaly, as it would be too old. New field research regarding the Orosei-Dorgali tidal notch underlines the younger timing for some of the Dorgali-Orosei volcanic deposits. In fact, new findings (Fig. 15) present evidence that one lava deposit near Cala Gonone covered and filled the lithophaga holes carved on the limestones MIS 5.5 double notch (Antonioli *et al.*, 2006) at an altitude of about 4 m. This observation leads us to state that some lavas are younger than 125 ka and consider the Dorgali-Orosei complex as a candidate for a volcanic load that could be responsible for the observed notch anomaly.

So as to study the effect of a volcanic load on the vertical movement of the coast, we first considered the flexure due to synthetic loads that resemble the features of a Sardinian volcanic load. Regarding the flexural modelling, one parameter that affects the solutions is the flexural rigidity. Presently this parameter is unknown for this area and would require a separate study to be determined (e.g., Braitenberg *et al.*, 2003, 2006; Ebbing *et al.*, 2007; Wienecke *et al.*, 2007). We have therefore investigated the flexural response assuming different rigidities.

We find that the volcanic loads cannot reproduce the local bulge needed to explain the uplift in the Orosei Gulf outlined by the observation of the MIS 5.5 anomalies (Figs. 11,

Figure 15
1) The base of the large smoothed notch near Cala Gonone carved into the limestone, with eroded but still well-preserved Lithophaga holes; 2) the explosive portion of the lava flow (volcanic breccia); 3) The basalt; 4) The lithophaga holes filled with black volcanic rock.

12). We then used the model of a spherical overpressure source (Mogi, 1958) and an alternative model for which an uplift is linked to the intrusion of a magmatic body (laccolith/batholith), following the model proposed by Turcotte and Schubert (2002) and the theory of which is found in more general terms in Timoschenko and Woinowsky-Krieger (1959).

We find that the Mogi-model cannot explain the anomaly, due to the fact that the wavelength of the anomaly is too small. The laccolith/batholith model, however, gives satisfactory results and can explain the anomaly. We find a class of possible solutions, with the parameters of plate radius (a), dyke radius (b), and pressure value (P) being in the ranges: $a = 40-50$ km, $b = 0.32-0.37$ km, $P = 0.27-0.28$ GPa. The plate radius of the laccolith/batholith model defines the radius of the area that is affected by the uplift with the borders of the area being supported by the underlying strata. The geographical position of the laccolith centers are located in an area near Punta Nera d'Osalla. The range of possible positions for the source corresponds to a sector that extends from Orosei to the offshore volcanic deposit. A more southern position, e.g., at Biddiriscottai near Cala Gonone, where from a geomorphological standpoint the basalt fills the tidal notch, indicating a younger age, would not be acceptable as a position of the overpressure source. Nonetheless a plausible model could involve local uplift due to magmatic intrusion that produced some basalt products that reached the surface.

7. Conclusion

In the present study we have attempted to explain a height anomaly of the MIS 5.5 tidal notch in a presently tectonically stable area: the Sardinia Island. Our results show

that the surface volcanic loads cannot be responsible for the notch level anomaly because the two possible load candidates when considering the ages of the volcanic deposits, the Dorgali-Orosei and the Logudoro volcanic units, have been shown to not produce coastal uplift. Another model that has been used to describe the updoming is the Mogi-model (Mogi, 1958). We find that this also does not explain the anomaly. In fact, in the "Mogi model," the flexure wavelength linked to a plausible source is smaller than the observed anomaly. In order to increase the characteristic wavelength the depth of the pressure source would have to be increased to unacceptable values, in that it would need to be located below the crust.

The third model we considered is that of a magmatic intrusion. The position of the source of the intrusion could be located between Punta Nera d'Osalla and a submarine volcanic deposit (Orrù, 2004). We find that a magmatic intrusion modelled by an overpressure over a circular area applied to an elastic layer can explain the observations. If our assumptions are correct, this result would have the consequence that the most recent documented volcanic activity (Logudoro volcanic units, in western Sardinia) aged between 0.1 ka and 0.4 ka according to different authors was not confined to western Sardinia, but also affected the eastern part of Sardinia. The activity to the east would have mainly produced a magmatic intrusion, with reduced or absent volcanic products at the surface, with evidence of young basaltic products to the east proposed from geomorphologic observations. This last hypothesis can be confirmed only with new data that consider the dates and geochemistry of the basalts. Given the importance of the issue, the need for more geological investigations and good and more extensive radiometric ages is evident.

Presently, we have unequivocal evidence that young basaltic products cover and fill the MIS 5.5 tidal notch and lithophaga holes near Cala Gonone (Fig. 15). This observation cannot be explained if the basaltic products were older than the age at which the notch was formed. According to our flexural modelling, these deposits could be associated with the intrusion that produced the coastal localized uplift. These basaltic deposits are of too small volume to have produced a considerable downward deformation of the MIS 5.5 notch, with the uplift due to the intrusion being the predominant effect. Our conclusion, that the western Sardinia coast was also affected by relatively young volcanism, opens new prospects in the understanding of this stable area of the Mediterranean.

Acknowledgements

We thank Egidio Trainito and Paolo Orru' for assistance in the geomorphological surveys, and Riccardo Petrini, Gabriella Demarchi and Stefano Furlani for helpful discussions. Kevin Fleming and an anonymous reviewer are thanked for their meticulous reviews and valuable suggestions.

References

Antonioli, F. and Trainito, E. (2005), *I solchi di battente di Tavolara e del Golfo di Orosei in Sardegna: nuovi dati e loro significato paleoambientale*, Atti congresso Marevivo, Olbia, novembre 2005, Posters.

Antonioli, F., Silenzi, S., Vittori, E., and Villani, C. (1999), *Sea-level change and tectonic mobility: precise measurement in three coastlines of Italy considered stable during the last 125 ky*, Phys. Chem. Earth. *24*, 337–342.

Antonioli, F., Kershaw, S., and Ferranti, L. (2006), *A double MIS 5.5 marine notch?* Quat. Int. 145-146, 19–29.

Assorgia, A., Beccaluva, L., Di Paola, G., Maccioni, G., Macciotta, G., Puxeddu, M., Santacroce R., and Venturelli, G. (1976), *Il complesso vulcanico di Monte Arci (Sardegna centro-occidentale), Nota illustrativa alla carta geopetrografica 1:50.000*, Boll. Soc. Geol. It. *95*, 371–401.

Assorgia, A., Barca, S., and Spano, C. (1997), *A synthesis on the Cenozoic stratigraphic, tectonic and volcanic evolution in Sardinia (Italy)*, Boll. Soc. Geol. It. *116*, 407–420.

Beccaluva, L., Macciotta, G., and Venturelli, G. (1975), *Dati geochimici e petrografici sulle vulcaniti Plio-Quaternarie della Sardegna centro-occidentale*, Boll. Soc. Geol. It. *94*, 1437–1457.

Beccaluva, L., Macciotta, G., and Venturelli, G. (1976), *Le vulcaniti Plio-Quaternarie del Logudoro (Sardegna nord-occidentale)*, Boll. Soc. Geol. It. *95*, 339–350.

Beccaluva, L., Deriu, M., Macciotta, G., Savelli, G., and Venturelli, G. (1977), *Geochronology and magmatic characters of the Pliocene-Pleistocene Volcanism in Sardinia (Italy)*, Bull. Volcanol. *40*, 154–168.

Beccaluva, L., Civetta, L., Macciotta, G., and Ricci, C. A. (1985), *Geochronology in Sardinia: Results and problems*, Rend. Soc. It. Mineral. Petrol. *40*, 57–72.

Beccaluva, L., Bianchini, G., and Siena, F. (2004), *Tertiary-Quaternary Volcanism and Tectono-Magmatic Evolution in Italy*, Special Volume of the Italian Geological Society for the IGC 32 Florence 2004, 153–160.

Belluomini, G., Discendenti, A., Malipieri, L., and Nicoletti, M. (1970), *Studi sulle ossidiane italiane II. Contenuto in ^{40}Ar radiogenico e possibilità di datazione*, Per. Min. *34*, 469–479.

Bigazzi, G., Bonadonna, P. F., Belluomini, G., and Malipieri, L. (1971), *Studi sulle ossidiane italiane. IV. Datazione con il metodo delle tracce di fissione*, Boll. Soc. Geol. It. *90*, 469–480.

Bigi, G. Cosentino, D., Parotto, M., Sartori, R., and Scandone, P. (1992), *Structural model of Italy*. Consiglio Nazionale delle Ricerche (CNR) – 1:500 000. Florence, Italy.

Braitenberg, C., Wang, Y., Fang, J., and Hsu, H. T. (2003), *Spatial variations of flexure parameters over the Tibet-Quinghai plateau*, Earth Planet. Sci. Lett. *205*, 211–224.

Braitenberg, C., Wienecke, S., and Wang, Y. (2006), *Basement structures from satellite-derived gravity fied: South Cina Sea ridge*, J. Geophys. Res. *111*, B05407.

Carmignani, L., Carosi, R., Disperati, T., Funedda, A., Musumeci, G., Pasci, S., and Pertusati, P. C., *Tertiary transpressional tectonics in NE Sardina, Italy*. In *Contributions to the Geology of Italy with Special Regard to the Paleozoic Basements*, IGCP No. 276 Newsletter 5, 83-96 (eds. Carmignani L. and Sassi F. P.), (Siena, 1992).

Carmignani, L., Barca, S., Disperati, L., Fantozzi, P., Funedda, A., Oggiano, G., and Pasci, S. (1994), *Tertiary compression and extension in the Sardinian basement*, Boll. Geof. Theor. Appl. *36*, 45–62.

Carmignani, L, Decandia, F. A., Disperati, L., Fantozzi, P. L., Lazzaretto, A., Lotta, D., and Oggiano, G. (1995), *Relationship between the Tertiary evolution of the Sardinia-Corsica-Provençal Domain and the Northern Apennines*, Terra Nova *7*, 128–137.

Carmignani, L., Conti, P., Cornamusini, G., and Mecchieri, M. (2004), *The internal Northern Apennines, the nothern Tyrrhennian Sea and the Sardinia-Corsica block*, Special Volume of the Italian Geological Society for the IGC 32 Florence 2004, 59-77.

Casula, G., Cerchi, A., Montadert, L., Murru, M., and Sartia, E. (2001), *The Cenozoic graben system of Sardinia (Italy): geodynamic evolution from new seismic and field data*, Marine Petro. Geol. *18*, 863–888.

Cocozza T., Jacobacci, A., Nardi, R., and Salvatori, I. (1974), *Schema stratigrafico strutturale del Massiccio Sardo-Corso e mineralogenesi della Sardegna*, Mem. Soc. Geol. It. *13*, 85–186.

Conti P., Eltrudis, A., Funedda, A., Pasci, S., Barca, S., Carmignani, L., Oggiano, G., Pertusati, P. C., and Salvatori, I. (1996), *Carta geologica della Sardegna, Scala 1:200000*, Servizio Geologico Nazionale e

Regione Autonoma della Sardegna. A cura del comitato per il coordinamento della Cartografia Geologica e Geotermica della Sardegna.

DBMI04, (2007), http://emidius.mi.ingv.it/DBMI04/.

Di Battistini, G., Montanini, A., and Zerbi, M. (1990), *Geochemistry of volcanic rocks from south-eastern Montiferro*, Neues. Jahrbuch Mineral. Abh. *162*, 35–67.

Di Paola, G. M., Puxxeddu, M., and Santacroce, R. (1975), *K/Ar age of Monte Arci volcanic complex (central-weastern Sardinia)*, Rend. SIMP. *31*, 101–109.

Ebbing, J., Braitenberg, C., and Wienecke, S. (2007), *Insights into the lithospheric structure and the tectonic setting of the Barents Sea region from isostatic considerations*, Geophys. J.Int. *171*, 1390–1403, doi: 10.1111/j.1365-246X.2007.03602.x.

Farr, T. G.*et al*. (2007), *The Shuttle Radar Topography Mission*, Rev. Geophys. *45*, RG2004, doi:10.1029/2005RG000183.

Fernandez, J. and Rundle, J. B. (1994), *Gravity change and deformation due to magmatic intrusion in two-layered crustal model*, J. Geoph. Res. *99*, 2737–2746.

Ferranti, L., Antonioli, F., Mauz, B., Amorosi, A., Dai Pra, G., Mastronuzzi, G., Monaco C., Orrù, P., Pappalardo, M., Radtke, U., Renda, P., Romano, P., Sansò, P., and Verrubbi, V. (2006), *Markers of the last interglacial sea-level high stand along the coast of Italy: Tectonic implications*, Contributions from the 32nd IGC, Ed. Quaternary Internat. *145–146*, 30–54.

Finetti, I. R., Del Ben, A., Fais, S., Forlin, E., Klingelé, E., Lecca, L., Pipan, M., Prizzon, A., *Crustal tectono-stratigraphic setting and geodynamics of the corso-Sardinian block from crop seismic data*. In *Crop Project: deep seismic exploration of the Central Mediterranean and Italy* (Elsevier, 1995), pp. 413–446.

Gueguen, E., Doglioni, C., and Fernández, M. (1998), *On the post-25 Ma geodynamic evolution of the western Mediterranean*, Tectonophysics *298*, 259–269.

INGV (2007), http://ingv.it/.

Kastens, K., Mascle, J., and others (1988), *ODP Leg 107 in the Tyrrhenian Sea: Insights into passive margin and back-arc basin evolution*, Geol. Soc. Am. Bull. *100*, 1140–1156.

Kershaw, S. and Antonioli, F. (2004), *Tidal notches at Taormina, east Sicily: Why is the mid-Holocene notch well-formed, but no modern notch is present in the same locality?* Quaternaria Nova VIII, 155–170.

Lambeck, K., Antonioli, F., Purcell, A., and Silenzi, S. (2004a), *Sea level change along the Italian coast for the past 10 000 yrs*, Quaternary Sci. Rev. *23*, 1567–1598.

Lambeck, K., Antonioli, F., Purcell, A., and Stirling, C. (2004b), *MIS 5.5 Sea level in the Mediterranean and inferences on the global ice volumes during late MIS 6 and MIS 5.5*. In *Proce. 32nd Internat. Geol. Congress*, Florence. Italy.

Love, A. E., *A treatise on the Mathematical Theory of Elasticity* (Dover Publications, New York 1944), 643 pp.

Lustrino, M. (1999), *Petrogenesis of Plio-Quaternary rocks from Sardinia: Possible implication on the evolution of the European subcontinental mantle*, Ph.D. Thesis, Università di Napoli Federico II, pp. 188.

Lustrino, M. (2000a), *Volcanic activity during the Neogene to Present evolution of the western* Mediterranean area: review, Ofioliti 25, 87-101.

Lustrino, M. (2000b), *Phanerozoic geodynamic evolution of the circum-Italian realm*, Int. Geol. Rev. *42*, 724–757.

Lustrino, M. (2000c), *Petrogenesis of tholeiitic volcanic rocks from central-southern Sardinia*, Mineral. Petrogr. Acta *43*, 1–16.

Lustrino, M., Melluso, L., Morra, V., and Secchi, F. (1996), *Petrology of Plio-Quaternary rocks from central Sardinia*, Per. Min. *65*, 275–287.

Lustrino, M., Melluso, L., and Morra, V. (2000), *The role of lower continental crust and lithospheric mantle in the genesis of Plio-Pleistocene volcanic rocks from Sardinia (Italy)*, Earth Plan. Sci. Lett. *180*, 259–270.

Lustrino, M., Melluso, L., and Morra, V. (2002), *The transition from alkaline to tholeiitic magmas: A case study from the Orosei-Dorgali Pliocene volcanic district (NE Sardinia, Italy)*, Lithos *63*, 83–113.

Lustrino, M., Melluso L., Morra, V., Brotzu, P., D'Amelio, F., Fedele, L., Franciosi, L., Leonis, R., and Petteruti Lieberknecht, A. M. (2004), *The Cenozoic igneous activity of Sardinia*., Per. Mineral., 73 (1), 105–134.

Lustrino, M., Morra, V., Fedele, L., and Serracino, M., (2007a), *The transition between "orogenic" and "anorogenic" magmatism in the western Mediterranean area. A case study from the Late Miocene volcanic rocks of Isola del Toro (SW Sardinia, Italy)*, Terra Nova *19*, 148–159.

Lustrino, M., Melluso, L., and Morra, V., (2007b), *The geochemical peculiarity of "Plio-Quaternary" volcanic rocks of Sardinia in the circum-Mediterranean Cenozoic Igneous Province*. In *Cenozoic volcanism in the Mediterranean area*, (Beccaluva L., Bianchini G., Wilson M. Eds. 2007), Geol. Soc. Am. Spec. Pap. *418*, 277–301.

Mascle, J. and Rehault J. P., *A revised stratigraphy of the Tyrrhenian sea: Implications for the basin evolution. In* Proc. Ocean Drilling Program, Scientific Results (eds. Kastens K. A. and Muscle J.), (College Station, TX 1990), *107*, 617–636.

Mogi, K. (1958), *Relations between the eruptions of various volcanoes and the deformations of the ground surfaces around them*, Bull. of the Earthq. Res. Inst. *36*, 99–134.

Montanini, A., Barbieri, M., and Castorina, F. (1994), *The role of fractional crystallization, crustal melting and magma mixing in the petrogenesis of rhyolites and mafic inclusion-bearing dacites from the Monte Arci volcanic complex (Sardinia, Italy)*, J. Volcanol. Geotherm. Res. *61*, 95–120.

NEIC (2007), http://neic.usgs.gov/neis/sopar/.

Nicolich, R. (2001), *Deep seismic transect*. In *Anatomy of an Orogen: The Apennines and the Adjacent Mediterranean Basins* (eds. Vai G. B. and Martini I. P.), (Kluwer Academic Publishers, Dordrecht, The Netherlands 2001), pp. 47–52.

Nicolich, R. and Dal Piaz, G. V. (1992), *Moho isobaths. Structural model of Italy. Scale 1: 500,000*, Quaderni de "La ricerca scientifica" *114* (3), CNR.

Orrù, P. (2004), *Morfologie sommerse*, Morfologia Costiera, Tav. 34. In *Atlante dei tipi geografici, (Istituto Geografico Militare editor)*, pp. 868. ISBN: 88-523-8913-X. Online: http://www.igmi.org/pubblicazioni/atlante_tipi_geografici/consulta_atlante.php.

Panza, G. F., Peccerillo, A., Aoudia, A., and Farina, B. (2007), *Geophysical and petrological modelling of the structure and composition of the crust and upper mantle in complex geodynamic settings: The Tyrrhenian Sea and surroundings*, Earth Sci. Rev. *80*, 1–46.

Pasci, S. (1997), *Tertiary transcurrent tectonics of North-Central Sardinia*, Bull. Soc. Gèol. France *168*, 301–312.

Patacca, E., Sartori, R., and Scandone, P. (1990), *Thyrrhenian basin and Apenninic arcs: Kinematic relations since late Tortonian times*, Mem. Soc. Geol. It. *45*, 425–451.

Petteruti Lieberknecht, A. M., Fedele, L., D'Amelio, F., Lustrino, M., Melluso, M., and Morra V. (2003), *Plio-Pleistocene igneous activity in Sardinia (Italy)*, Geophys. Res. Abstract Vol. 5, 07260, European Geophysical Society.

Sartori, R., Leg OPD 107 Scientific Staff. *Drillings of OPD Leg 107 in the Thyrrenian sea: tentative basin evolution compared to deformations in the surronding chain*. In *The Lithosphere in Italy* (Boriani, A., Bonafede, M, Piccardo, G. B., and Vai, G. B., eds), (Accademia dei Lincei, Roma, 1989), pp. 139–156.

Savelli, C. (1975), *Datazioni preliminari con il metodo K-Ar sulle vulcaniti della Sardegna*, Rend**.** Soc. It. Min. Petrol. *31*, 191–198.

Savelli, C. and Pasini, G. (1973), *Preliminary results of K-Ar dating of basalts from eastern Sardinia and Gulf Orosei (Tyrrhenian Sea)*, Giorn. di Geol. *39* (1), 303–312.

Scrocca, D., Doglioni C., and Innocenti, F. (2003), *Constraints for an interpretation of the Italian geodynamics: a review*, Mem. Descr. Carta Geol. d'It. LXII, 15–46.

Speranza, F. (1999), *Paleomagnetism and the Corsica–Sardinia rotation: A short review*, Boll. Soc. Geol. Ital. *118*, 537–543.

Speranza, F., Villa, I. M., Cagnotti, L., Florindo, F., Casentino, D., Cipollati, P., and Mattei, M. (2002), *Age of the Corsica-Sardinia rotation and Liguro-Provençal basin spreading: New paleomagnetic and Ar/Ar evidence*, Thect. *347*, 231–251.

Timoshenko, S. P. and Woinowsky-Krieger, S., *Theory of Plates and Shells* (McGraw-Hill International Edition, (1959) Engineering Mechanics Series, Second edition), 580 pp.

Turcotte, D. L. and Schubert, G., Geodynamics, (Cambridge University Press, 2002), 456 pp.

Watts, A. B., *Isostasy and Flexure of the lithosphere* (Cambridge University Press, 2002), 459 pp.

WIENECKE, S., BRAITENBERG, C., and GÖTZE, H.-J. (2007), *A new analytical solution estimating the flexural rigidity in the Central Andes*, Geophys. J. Int., *169*, 789–794, doi:10.1111/j.1365-246X.2007.3396.x.

(Received February 22, 2008, revised December 18, 2008, accepted January 11, 2009)
Published Online First: June 27, 2009